J. Fluid Mech. (2000), *vol.* 403, *pp.* 173–199. Printed in the United Kingdom

Transonic flow of moist air around a thin airfoil with non-equilibrium and homogeneous condensation

By ZVI RUSAK AND JANG-CHANG LEE

Department of Mechanical Engineering, Aeronautical Engineering and Mechanics, Rensselaer Polytechnic Institute, Troy, NY 12180-3590, USA

(Received 5 March 1999 and in revised form 8 September 1999)

A new small-disturbance model for a steady transonic flow of moist air with non-equilibrium and homogeneous condensation around a thin airfoil is presented. The model explores the nonlinear interactions among the near-sonic speed of the flow, the small thickness ratio and angle of attack of the airfoil, and the small amount of water vapour in the air. The condensation rate is calculated according to classical nucleation and droplet growth models. The asymptotic analysis gives the similarity parameters that govern the flow problem. Also, the flow field can be described by a non-homogeneous (extended) transonic small-disturbance (TSD) equation coupled with a set of four ordinary differential equations for the calculation of the condensate (or sublimate) mass fraction. An iterative numerical scheme which combines Murman & Cole's (1971) method for the solution of the TSD equation with Simpson's integration rule for the estimation of the condensate mass production is developed. The results show good agreement with available numerical simulations using the inviscid fluid flow equations. The model is used to study the effects of humidity and of energy supply from condensation on the aerodynamic performance of airfoils.

1. Introduction

The compressible dynamics of atmospheric humid air around airfoils and wings is a fundamental scientific problem of interest which also has important technological applications in the design of airplanes, helicopters, compressors, turbines, nozzles, shock tubes, and cryogenic wind tunnels. Once the condensation of the water vapour in moist air takes place, liquid droplets nucleate. The condensation process releases heat to the surrounding gaseous components of moist air and significantly affects their thermodynamic and flow properties (see, for example, Wegener & Mack 1958 who investigated shock wave solutions with heat transfer). As a result, variations in the aerodynamic performance of the airfoils can be found (Schnerr & Dohrmann 1990, 1994).

The transonic flow of moist air has been studied by Head (1949), Schmidt (1966), Zierep (1971), Jordan (1972), Hall (1979), Campbell, Chambers & Rumsey (1989), and Schnerr & Dohrmann (1990, 1994). When the flow approaches the nose region of the airfoil, it decelerates to stagnation, the local pressure and temperature increase, and the relative humidity, Φ, decreases. Here $\Phi = p_v/p_g(T) \leqslant 1$ where p_v is the local vapour pressure and $p_g(T)$ is the saturation pressure of water vapour at the temperature T of the local flow. When the flow expands around the nose of the airfoil, its speed increases. From the conservation of momentum and energy, the local pressure and

temperature decrease and the relative humidity increases. In most relevant cases of transonic flows humid air reaches the saturation conditions ($\Phi = 100\%$) and the condensation of water vapour in the air may occur.

The condensation may develop in one of two possible limit types of processes (Wegener 1975). The first type is an equilibrium process which typically occurs in flows where the changes of state are relatively 'slow' and there are large numbers of condensation nuclei. In this process the condensation starts immediately water vapour reaches the saturation conditions and it may be modelled as an isentropic process that evolves according to the local flow properties. The second possible type of behaviour is a non-equilibrium process, which usually happens in rapid expansions of highly purified vapours in supersonic nozzles and around airfoils in cloud chambers. In this process the supersaturation ratio $S = p_v/p_g(T) > 1$ (see, for example, Zettlemoyer 1969 and Abraham 1974) may increase much above one ($S \gg 1$) without condensation because the liquid droplets do not reach the critical size for growth and collapse back to water vapour. At the critical state, known as a supersaturation state, the liquid droplets reach the critical size. A significant nucleation of water droplets is suddenly initiated by spontaneous fluctuations in the water vapour itself, known as homogeneous condensation. This process takes place along a relatively short distance, on the order of several percent of the airfoil's chord. In certain situations a condensation compression wave is formed (see Wegener & Mack 1958). Experiments show that the non-equilibrium process happens in transonic wind tunnels operating with atmospheric humid air such as in the French tunnel S1 at Modane (G. H. Schnerr, private communication). On the other hand, the equilibrium process usually takes place in atmospheric transonic flight.

The transonic flow around the airfoil also contains a regular shock wave. The pressure and temperature of the flow behind the shock wave must increase and, as a result, the liquid droplets may partially evaporate. It is usually assumed that the evaporation process is governed by the same rules as condensation (see, for example, Schnerr & Dohrmann 1990, 1994).

The heat transfer as a result of the condensation or evaporation of moist air affects the flow properties, specifically the pressure distribution along the surfaces of the airfoil. At transonic speeds where shock waves appear, the condensation alters the flow properties ahead of the shock wave and affects its position and strength. In certain cases, the structure of the entire supersonic flow region around the airfoil is changed and a steady double shock system may appear (see Zierep 1969 for theoretical considerations and Head (1949) and Schnerr & Dohrmann (1990, 1994) for experimental and computational examples of such situations). Therefore, the aerodynamic performance of the airfoil such as the lift, drag, and pitching moment coefficients are changed when the relative humidity of the oncoming stream varies. For example, through numerical computations using the inviscid flow equations with a heat addition term and a nucleation model, Schnerr & Dohrmann (1990, 1994) demonstrated significant changes in the lift and drag coefficients of various airfoils as function of the relative humidity at the stagnation conditions.

In this paper we concentrate on transonic flows of moist air around a thin airfoil with non-equilibrium and homogeneous condensation. The thermodynamic behaviour of such a condensation process is the subject of Wegener & Mack (1958), Wegener & Pouring (1964), Hill (1966), Wegener (1975), Peters (1983), and Peters & Paikert (1989). These papers provide experimental data and theoretical considerations which describe this complicated process of water vapour phase change. A review of the classical theory of nucleation and condensation of water vapour according to Wegener

& Mack (1958) and Hill (1966) is provided in Appendix A. The equations which describe the nucleation rate J, the critical droplet size r^*, the droplet growth rate $\mathrm{d}r/\mathrm{d}t$, and the rate of change of the condensate mass fraction g are shown. This theory (equations (A 1)–(A 5)) will be used in the present analysis.

The effect of heat transfer to or from the flow on possible shock wave solutions in a transonic or supersonic flow was first studied by Wegener & Mack (1958). Through a model equation, they demonstrated the possible existence of condensation shock waves and of exothermic jumps in subsonic flows in addition to modified regular shock waves with either condensation or vaporization.

Zierep (1969) developed a modified transonic small-disturbance model equation for a flow around a thin airfoil which includes a prescribed heat source term to represent the heat release by condensation. Through simplifying assumptions, he derived approximate solutions of this problem for various prescribed values of the heat input. He found a critical heat input, which is related to the dry air solution, above which no steady solution exists. He also showed the possible reduction of the airfoil's drag as a result of a heat input in the supersonic part of the flow field. Schnerr & Mundinger (1993) used Zierep's (1969) model together with prescribed distributions of heat sources which simulate the essential features of non-equilibrium condensation. They derived similarity parameters that may govern transonic flow behaviour with internal heat addition. They also investigated the changes in aerodynamic lift and drag of airfoils resulting from the heat addition.

Schnerr & Dohrmann (1990, 1994) have conducted extensive numerical simulations of transonic flows of moist air around airfoils. Their calculations were based on the Euler equations of motion with a heat source term caused by condensation and related to the condensate mass fraction. The classical theory of Wegener & Mack (1958) and Hill (1966) described in Appendix A was used to determine the nucleation rate J, the droplet growth rate $\mathrm{d}r/\mathrm{d}t$, and the condensate mass fraction g. Specifically, Hill's (1966) equation for the rate of change of g (equation (A 5)) was transformed to an unsteady system of partial differential equations to compute the field of g. The system of the conservation and condensation equations was solved by a time-dependent and explicit finite volume method. Using this model, they studied various transonic flows of moist air around airfoils and described the variation of the pressure distribution due to a heat supply by condensation. Depending on the airfoil's geometry and different supply conditions, they showed significant variations of the lift and pressure drag that may amount to an increase or, sometimes, decrease of about 50% or more compared to the dry air flow case at the same Mach number.

The review of the previous work shows that transonic flows of moist air around airfoils may create complicated flow fields which are quite different from the classical dry air flow case and may result in significant changes in the aerodynamic performances of the airfoils. The study of this problem has focused over the years on experimental investigations and numerical simulations. A theoretical asymptotic analysis that simplifies the flow and condensation equations may shed more light on the problem and add to our understanding of the complicated compressible flow physics of moist air.

In the present paper we develop a small-disturbance model for a steady transonic flow of moist air with a non-equilibrium and homogeneous condensation around a thin airfoil. The outline of the paper is as follows. The mathematical model of the flow problem is described in § 2. The condensation rate is calculated according to the classical nucleation and droplet growth models of Wegener & Mack (1958) and Hill (1966) (see Appendices A and B). The asymptotic analysis in § 3 explores the

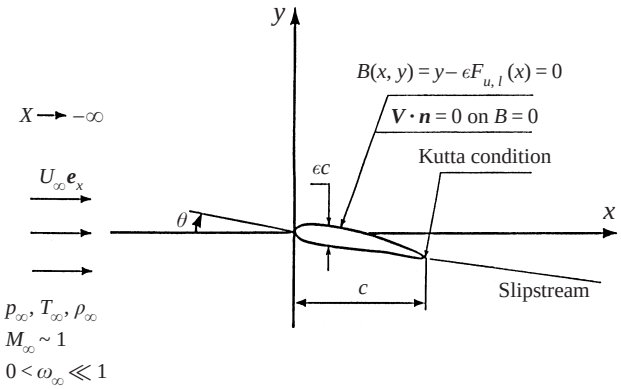

FIGURE 1. Airfoil flow problem.

nonlinear interactions between the near sonic speed of the flow, the small thickness and angle of attack of the airfoil, and the small amount of water vapour in the air. It gives the similarity parameters which govern the flow problem. Also, the flow field can be described by a non-homogeneous (extended) transonic small-disturbance (TSD) equation coupled with a set of four ordinary differential equations for the calculation of the condensate (or sublimate) mass fraction. This approach extends the classical TSD problem for dry air (see, for example, Cole & Cook 1986) and the works of Zierep (1969) and Schnerr & Mundinger (1993) where the heat addition is prescribed. In the present work the heat addition results from the model equations for the condensation process. An iterative numerical scheme which combines Murman & Cole's (1971) method for the solution of the modified TSD equation with Simpson's integration rule for the computation of the condensate mass fraction field is developed in § 4. The results in § 5 show good agreement with available numerical simulations using the Euler equations. The model is used to study the effects of humidity and of energy supply by condensation on the aerodynamic performances of airfoils.

2. Mathematical model

For many practical applications, moist air of the atmosphere is considered as a mixture of perfect gases. It is composed of clean dry air of constant composition and water vapour, where dry air is not condensible and water vapour is condensible (see Wegener & Pouring 1964). Moist air behaves as a thermally perfect gas and each of the gaseous components of moist air is also a thermally and calorically perfect gas (constant specific heat coefficients). This mixture also satisfies Dalton's law of partial pressures, i.e. each component of the mixture behaves as a perfect gas as if it were alone at the temperature, T, and the volume, V, of the mixture. The total pressure of the mixture, p, equals the sum of the partial pressure of each component. When the condensation of water vapour in the air takes place, the molecular weight and specific heat coefficients of the gaseous mixture may change. Moreover, the heat addition caused by the condensation process affects the thermodynamic and dynamic properties of the flow.

A steady, inviscid, and two-dimensional transonic flow of moist air around a thin airfoil is considered in an (x, y)-plane (figure 1). The flow far ahead of the airfoil is assumed to be uniform at a speed U_∞ in the axial direction only, pressure p_∞, density ρ_∞, temperature T_∞, and supersaturation ratio $S_\infty > 1$ (or relative humidity

$0 \leqslant \Phi_\infty \leqslant 100\%$). The flow speed U_∞ is close to the isentropic speed of sound, a_∞, of the upstream moist air at the given conditions, i.e. the frozen free-stream Mach number $M_\infty = U_\infty/a_\infty \sim 1$. Here, $a_\infty = \sqrt{\gamma_\infty R_\infty T_\infty}$ where the ratio of specific heats, γ_∞, and the specific gas constant, R_∞, of moist air are given by

$$\gamma_\infty = \frac{C_{p\infty}}{C_{v\infty}} = \frac{(1-\omega_\infty)C_{pa} + \omega_\infty C_{pv}}{(1-\omega_\infty)C_{va} + \omega_\infty C_{vv}} = \gamma_a \frac{1-\omega_\infty + \omega_\infty \tilde{C}_p}{1-\omega_\infty + \omega_\infty \tilde{C}_v}, \tag{1}$$

$$R_\infty = \frac{\bar{R}}{\mu_\infty}. \tag{2}$$

Here $\bar{R}$ is the universal gas constant, $1/\mu_\infty = (1-\omega_\infty)/\mu_a + \omega_\infty/\mu_v$ and μ_∞ is the apparent molecular weight of the upstream moist air, and μ_a and μ_v are the molecular weights of dry air and water, respectively. Also, $\omega_\infty = [\rho_v/(\rho_a+\rho_v)]_\infty = \chi_\infty/(1+\chi_\infty)$ (where ρ_a is the dry air density) is the initial specific humidity at the upstream state and

$$\chi_\infty = \frac{\rho_v}{\rho_a}\bigg|_\infty = \frac{\mu_v}{\mu_a}\frac{p_g(T_\infty)S_\infty}{p_\infty - p_g(T_\infty)S_\infty}$$

is the humidity ratio (or the mixing ratio) of the upstream flow. Also in (1), $\gamma_a = C_{pa}/C_{va}$ is the ratio of specific heats of dry air. C_{pa} and C_{va} are the specific heats at constant pressure and volume of dry air, respectively. C_{pv} and C_{vv} are those of water vapour when it is approximated as a perfect gas. $\tilde{C}_p = C_{pv}/C_{pa}$ and $\tilde{C}_v = C_{vv}/C_{va}$. Since typically $p_g(T_\infty) \ll p_\infty$, each particle of moist air contains a small amount of water vapour, $\omega_\infty \ll 1$. It is assumed that no condensation takes place at the upstream state, i.e. the condensate mass fraction $g_\infty = 0$ as $x \to -\infty$. We also assume that there is no injection of water vapour or liquid to the flow through the airfoil's surfaces.

The thin airfoil shape is given by

$$B(x,y) = y - \epsilon c F_{u,l}(x/c) = 0 \quad \text{for } 0 \leqslant x/c \leqslant 1, \tag{3}$$

where c is the chord, ϵ is the thickness ratio, and $0 < \epsilon \ll 1$. The functions $F_{u,l}(x/c)$ represent the upper and lower surfaces of the airfoil, respectively. These shape functions are given by

$$F_{u,l}(x/c) = Ca(x/c) \pm t(x/c) - \Theta x/c \quad \text{for } 0 \leqslant x/c \leqslant 1, \tag{4}$$

where $Ca(x/c)$ describes the camber line, $t(x/c)$ is the thickness distribution, and $\Theta = \theta/\epsilon$ where θ is the angle of attack. Also, $t(0) = t(1) = 0$ and $Ca(0) = Ca(1) = 0$.

Assuming the thermodynamic behaviour and dynamics of moist air as listed in Appendix A, the compressible flow field of humid air around the airfoil may be described by the conservation equations of mass, momentum, and energy:

$$(\rho u)_x + (\rho v)_y = 0, \tag{5}$$

$$(\rho u^2 + p)_x + (\rho uv)_y = 0, \tag{6}$$

$$(\rho uv)_x + (\rho v^2 + p)_y = 0, \tag{7}$$

$$(\rho h_T u)_x + (\rho h_T v)_y = 0. \tag{8}$$

Here p and ρ are the local pressure and density, u and v are the axial and transverse velocity components, h_T is the specific total enthalpy, and $\rho h_T = \frac{1}{2}\rho(u^2+v^2) + \rho_a h_a + \rho_v h_v + \rho_l h_l$. Also, we assume (see, for example, Moran & Shapiro 1992, pp. 82, 88,

103, and 583) that $h_a = C_{pa}T$, $h_v \sim h_g(T) = C_{pv}T$, and $h_l \sim h_f(T) = h_g(T) - h_{fg}(T)$ are the dry air, the water vapour, and the condensate specific enthalpies, respectively. Here h_g and h_f are the specific enthalpies of a saturated water vapour and liquid; h_{fg} is the latent heat resulting from the condensation of the water vapour into liquid.

We define the local density of a fluid particle as $\rho = \rho_a + \rho_v + \rho_l$, the local initial specific humidity as $\omega = (\rho_v + \rho_l)/\rho$ (where $0 < \omega \ll 1$), and the local condensate mass fraction as $g = \rho_l/\rho$ (where $0 < g < \omega$). We find that $\rho h_T = \frac{1}{2}\rho(u^2 + v^2) + \rho((1-\omega)C_{pa} + \omega C_{pv})T - \rho g h_{fg}$. Using (5) and (8) it can be shown that the specific total enthalpy, h_T, is constant along a constant stream function line ψ, where $\psi_y = \rho u$ and $\psi_x = -\rho v$. Therefore, the energy equation (8) becomes an algebraic relation:

$$\tfrac{1}{2}(u^2 + v^2) + ((1-\omega)C_{pa} + \omega C_{pv})T - g h_{fg} = h_T(\psi). \tag{9}$$

The equation of state for a thermally perfect gas is also considered, relating the local thermodynamic properties of moist air:

$$p = \frac{\bar{R}}{\mu}\rho T. \tag{10}$$

Here T is the local temperature and μ is the local apparent molecular weight of moist air, $1/\mu = (1-\omega)/\mu_a + (\omega - g)/\mu_v$.

Equations (5)–(7), (9), and (10) describe the flow field of moist air including the heat supply caused by the condensation process, which appears in the energy equation (9). Notice that the heat source term vanishes in flow regions with no condensation.

To compute the condensate mass fraction g, we assume the classical nucleation theory for a homogeneous condensation according to Volmer (1939), Wegener & Mack (1958), and Hill (1966) as described in Appendix A. Following Hill (1966), the condensate rate equation (A 5) can be generalized for a two-dimensional flow, resulting in

$$(\rho u g)_x + (\rho v g)_y = 4\pi\rho_l \left(\rho Q_1 \frac{\mathrm{d}r}{\mathrm{d}t} + \tfrac{1}{3} J r_0^3\right), \tag{11}$$

$$(\rho u Q_1)_x + (\rho v Q_1)_y = 2\rho Q_2 \frac{\mathrm{d}r}{\mathrm{d}t} + J r_0^2, \tag{12}$$

$$(\rho u Q_2)_x + (\rho v Q_2)_y = \rho Q_3 \frac{\mathrm{d}r}{\mathrm{d}t} + J r_0, \tag{13}$$

$$(\rho u Q_3)_x + (\rho v Q_3)_y = J. \tag{14}$$

Here, r_0 is the initial radius of a nucleus and according to Hill (1966) typically $r_0 = 1.3r^*$ (see the Thomson–Gibbs equation (A 2) for an estimation of r^*). Also, Q_1 is the sum of droplet surfaces per unit mass, Q_2 is the sum of droplet radii per unit mass, and Q_3 is the sum of droplets per unit mass. The nucleation rate J is given by (A 1) and (A 3), and the droplet growth rate $\mathrm{d}r/\mathrm{d}t$ by (A 4). In these equations, the saturation pressure of the water vapour $p_g(T)$, the water liquid density (approximated by the saturated liquid density $\rho_l = \rho_f(T)$), the surface tension of a plane surface $\sigma_\infty(T)$, and the condensation coefficient $\alpha(T)$, are all given thermodynamic functions of the temperature T (see, for example, Moran & Shapiro 1992; Schnerr & Dohrmann 1990, 1994, and Appendix B). The water vapour density ρ_v is found from the definitions of ω, g, and ρ:

$$\rho_v = \rho(\omega - g). \tag{15}$$

The water vapour pressure p_v is found from the perfect gas equations for both dry

air and water vapour ($p_a = \rho_a(\bar{R}/\mu_a)T$ and $p_v = \rho_v(\bar{R}/\mu_v)T$), Dalton's law of partial pressures for a mixture of perfect gases ($p = p_a + p_v$), and definitions of ω and g:

$$p_v = p\frac{\omega - g}{(\omega - g) + (1 - \omega)\mu_v/\mu_a}. \tag{16}$$

Equations (11)–(16) together with (A 1)–(A 4) describe the fields of the various parameters of the condensation process, specifically the condensate mass fraction g.

The system of flow equations (5)–(7), (9), and (10) coupled with the condensation equations (11)–(16) describes the flow field of steady and inviscid moist air with non-equilibrium and homogeneous condensation. The solution of these equations should satisfy the tangency boundary condition of the flow on the airfoil surface,

$$uB_x + vB_y = 0 \quad \text{on } B(x, y) = 0. \tag{17}$$

Also, disturbances to the uniform flow must die out at upstream infinity,

$$\left.\begin{array}{c} u \to U_\infty, \quad v \to 0, \quad \rho \to \rho_\infty, \quad p \to p_\infty, \\ g \to 0, \quad Q_1 \to 0, \quad Q_2 \to 0, \quad Q_3 \to 0 \quad \text{for all } y \text{ as } x \to -\infty. \end{array}\right\} \tag{18}$$

The Kutta condition must be satisfied at a sharp trailing edge. In order to get a one-valued flow field, the (x, y)-plane is cut along the slipstream that leaves the trailing edge to infinity.

Using the continuity equation (5), the relation $\rho = \rho_a/(1 - \omega)$, the fact that dry air and water in a fluid particle do not interact, and the uniform flow conditions at the upstream state, we find that the initial specific humidity is constant throughout the field, $\omega = \omega_\infty$ for all (x, y). This result is also correct across any shock wave that may appear in the flow. It reflects the conservation of the water mass at any point in the flow field.

Also, from the far-field conditions (18) we find that in the energy equation (9) $h_T(\psi)$ is constant throughout the field:

$$\tfrac{1}{2}(u^2 + v^2) + C_{p\infty}T - gh_{fg} = \tfrac{1}{2}U_\infty^2 + C_{p\infty}T_\infty, \tag{19}$$

for all (x, y). Here $C_{p\infty} = (1 - \omega_\infty)C_{pa} + \omega_\infty C_{pv}$. This result is also correct across any shock wave that may appear in the flow. It reflects the conservation of the specific total enthalpy at any point in the flow field.

In order to study the transonic flow of moist air around a thin airfoil, the flow and condensation properties are approximated by asymptotic expansions in the limit where the thickness ratio of the airfoil is small ($\epsilon \to 0$), the frozen free-stream Mach number is near 1 ($M_\infty \to 1$), and the initial specific humidity is also small ($\omega_\infty \to 0$).

3. Transonic small-disturbance theory for moist air

In the case of a transonic flow of a uniform stream of moist air around a thin airfoil, the upstream flow is characterized by a frozen Mach number that is close to 1 and by small values of the initial specific humidity. It is expected that the thin airfoil creates, in most of the flow field, only slight perturbations to the uniform flow properties, except for a small region near the nose of the airfoil (of the order of ϵ^2) where the perturbations are large. In order to describe the nonlinear interactions among the various perturbations we consider

$$M_\infty^2 = 1 - K\epsilon^\delta, \quad \omega_\infty = K_\omega \epsilon^\beta, \quad \bar{x} = \frac{x}{c}, \quad \tilde{y} = \epsilon^\nu \frac{y}{c}. \tag{20}$$

The terms K and K_ω are similarity parameters. The stretched coordinate $\tilde{y}$ is used because it is expected that in a transonic flow the perturbations spread over a large transverse distance from the airfoil in the y-direction. Also, using (A 2) and (A 4), we define the characteristic length and speed of the condensation process, $l_c = 2\sigma_\infty(T_\infty)/(\rho_{l\infty}R_v T_\infty)$ and $u_c = \omega_\infty(\rho_\infty/\rho_{l\infty})\sqrt{R_v T_\infty/2\pi}$, respectively. Here $\rho_{l\infty} = \rho_l(T_\infty)$. The flow and condensation properties may be approximated by

$$\left.\begin{aligned}
\bar{\rho} &= \frac{\rho}{\rho_\infty} = 1 + \epsilon^{a_1}\bar{\rho}_1 + \epsilon^{a_2}\bar{\rho}_2 + \cdots, \quad \bar{p} = \frac{p}{p_\infty} = 1 + \epsilon^{b_1}\bar{p}_1 + \epsilon^{b_2}\bar{p}_2 + \cdots, \\
\bar{T} &= \frac{T}{T_\infty} = 1 + \epsilon^{c_1}\bar{T}_1 + \epsilon^{c_2}\bar{T}_2 + \cdots, \\
\bar{u} &= \frac{u}{U_\infty} = 1 + \epsilon^{d_1}\bar{u}_1 + \epsilon^{d_2}\bar{u}_2 + \cdots, \quad \bar{v} = \frac{v}{U_\infty} = \epsilon^{e_1}\bar{v}_1 + \epsilon^{e_2}\bar{v}_2 + \cdots, \\
\bar{g} &= \frac{g}{\omega_\infty} = \epsilon^{f_1}\bar{g}_1 + \epsilon^{f_2}\bar{g}_2 + \cdots, \quad \bar{Q}_1 = \frac{Q_1}{\omega_\infty/\rho_{l\infty}l_c} = \epsilon^{l_1}\bar{Q}_{11} + \epsilon^{l_2}\bar{Q}_{12} + \cdots, \\
\bar{Q}_2 &= \frac{Q_2}{\omega_\infty/\rho_{l\infty}l_c^2} = \epsilon^{m_1}\bar{Q}_{21} + \epsilon^{m_2}\bar{Q}_{22} + \cdots, \\
\bar{Q}_3 &= \frac{Q_3}{\omega_\infty/\rho_{l\infty}l_c^3} = \epsilon^{n_1}\bar{Q}_{31} + \epsilon^{n_2}\bar{Q}_{32} + \cdots, \\
\bar{J} &= \frac{J}{\rho_\infty u_c/\rho_{l\infty}l_c^4},
\end{aligned}\right\} \tag{21}$$

where $0 \leqslant a_1 < a_2$ and similar relations apply to the other powers. The various perturbation functions with indices 1 and 2 in (21) are non-dimensional functions of $(\bar{x}, \tilde{y})$ and of the similarity parameters of the problem.

The substitution of (20) and (21) into the flow equations (5)–(7) and (9) provides the relations among the various powers: $a_1 = b_1 = c_1 = d_1$, $e_1 = b_1 + v$, $a_2 = b_2 = c_2 = d_2 = a_1 + d_1 = v + e_1 = d_1 + \delta$, and $e_2 = e_1 + a_1 = b_2 + v$. The value of the power β cannot be determined from these relations. However, from matching the effect of the condensate mass fraction in the term $1/\mu$ in the equation of state (10) with the pressure and density perturbations, it may be shown that $\beta + f_1 > a_1$ and, therefore, $\beta + f_1 = a_2$. From the boundary condition (17) and the given shape of the airfoil, it is found that $e_1 = 1$. Therefore, $v = \frac{1}{3}$, $a_1 = b_1 = c_1 = d_1 = \delta = \frac{2}{3}$, $a_2 = b_2 = c_2 = d_2 = \frac{4}{3}$, $e_2 = \frac{5}{3}$, and $\beta + f_1 = \frac{4}{3}$, as expected from the classical transonic small-disturbance theory for dry air (Cole & Cook 1986). From the condensation equations (11)–(14), we may also show that $f_1 = l_1 = m_1 = n_1 = 0$. Thus, $\beta = \frac{4}{3}$. Notice that $a_1 + \beta = 2$ and the terms of this order in (5)–(9) may be neglected. We find that $\tilde{y} = \epsilon^{1/3}y/c$, $\omega_\infty = \epsilon^{4/3}K_\omega$, $M_\infty^2 = 1 - K\epsilon^{2/3}$, and

$$\left.\begin{aligned}
\bar{\rho} &= 1 + \epsilon^{2/3}\bar{\rho}_1 + \epsilon^{4/3}\bar{\rho}_2 + \cdots, \quad \bar{p} = 1 + \epsilon^{2/3}\bar{p}_1 + \epsilon^{4/3}\bar{p}_2 + \cdots, \\
\bar{T} &= 1 + \epsilon^{2/3}\bar{T}_1 + \epsilon^{4/3}\bar{T}_2 + \cdots, \\
\bar{u} &= 1 + \epsilon^{2/3}\bar{u}_1 + \epsilon^{4/3}\bar{u}_2 + \cdots, \quad \bar{v} = \epsilon\bar{v}_1 + \epsilon^{5/3}\bar{v}_2 + \cdots, \\
\bar{g} &= \bar{g}_1 + \cdots, \quad \bar{Q}_1 = \bar{Q}_{11} + \cdots, \\
\bar{Q}_2 &= \bar{Q}_{21} + \cdots, \quad \bar{Q}_3 = \bar{Q}_{31} + \cdots.
\end{aligned}\right\} \tag{22}$$

Using $\omega_\infty = K_\omega\epsilon^{4/3}$, we find from (1) that $\gamma_\infty = \gamma_a[1 + K_\omega\epsilon^{4/3}(\tilde{C}_p - \tilde{C}_v) + \cdots]$. Also,

$h_{fg}(T) = h_{fg}(T_\infty) + O(\epsilon^{2/3})$ and $\rho_\infty U_\infty^2/p_\infty = \gamma_\infty M_\infty^2$. Substituting these expansions together with (22) into (5)–(7), (9), and (10) results in the equations relating the various perturbations:
from (5)

$$\epsilon^{2/3}(\bar{\rho}_1 + \bar{u}_1)_{\bar{x}} + \epsilon^{4/3}((\bar{\rho}_1\bar{u}_1 + \bar{\rho}_2 + \bar{u}_2)_{\bar{x}} + \bar{v}_{1\tilde{y}}) + \cdots = 0, \tag{23}$$

from (6)

$$\epsilon^{2/3}(\gamma_a M_\infty^2 \bar{u}_1 + \bar{p}_1)_{\bar{x}} + \epsilon^{2/3}\gamma_a M_\infty^2(\bar{\rho}_1 + \bar{u}_1)_{\bar{x}} + \epsilon^{4/3}\left[\left(\gamma_a M_\infty^2\left(\bar{\rho}_2 + 2\bar{u}_2 + \bar{u}_1^2 + 2\bar{\rho}_1\bar{u}_1\right) + \bar{p}_2\right)_{\bar{x}} + \gamma_a M_\infty^2 \bar{v}_{1\tilde{y}}\right] + \cdots = 0, \tag{24}$$

from (7)

$$\epsilon(\gamma_a M_\infty^2 \bar{v}_{1\bar{x}} + \bar{p}_{1\tilde{y}}) + \cdots = 0, \tag{25}$$

from (19)

$$\epsilon^{2/3}(\bar{T}_1 + (\gamma_a - 1)M_\infty^2 \bar{u}_1) + \epsilon^{4/3}\left[\bar{T}_2 + (\gamma_a - 1)M_\infty^2\left(\bar{u}_2 + \frac{\bar{u}_1^2}{2}\right) - \bar{g}_1 K_\omega \frac{h_{fg}(T_\infty)}{C_{pa}T_\infty}\right] + \cdots = 0, \tag{26}$$

and from (10)

$$\epsilon^{2/3}\left(\bar{p}_1 - \bar{\rho}_1 - \bar{T}_1\right) + \epsilon^{4/3}\left(\bar{p}_2 - \bar{\rho}_2 - \bar{T}_2 - \bar{\rho}_1\bar{T}_1 + \bar{g}_1 K_\omega \frac{\mu_a}{\mu_v}\right) + \cdots = 0. \tag{27}$$

Notice that in (23) and (24) we assume that $\epsilon^{2/3}(\bar{\rho}_1 + \bar{u}_1)$ may also be $O(\epsilon^{4/3})$.

Equation (24) shows that in the leading order $O(\epsilon^{2/3})$: $\gamma_a M_\infty^2 \bar{u}_1 + \bar{p}_1 = fn_1(\tilde{y})$. The function $fn_1(\tilde{y})$ must vanish according to the far-field conditions (18). Also, from (26), $\bar{T}_1 + (\gamma_a - 1)M_\infty^2 \bar{u}_1 = 0$ for all x and $\tilde{y}$. We find

$$\bar{p}_1 = -\gamma_a M_\infty^2 \bar{u}_1, \quad \bar{T}_1 = -(\gamma_a - 1)M_\infty^2 \bar{u}_1 \tag{28}$$

everywhere in the flow field, including across a shock wave. From (27), $\bar{\rho}_1 = \bar{p}_1 - \bar{T}_1$. Using (28), $\bar{\rho}_1 = -M_\infty^2 \bar{u}_1$. As a result, $\epsilon^{2/3}(\bar{\rho}_1 + \bar{u}_1) = \epsilon^{2/3}(1 - M_\infty^2)\bar{u}_1 = \epsilon^{4/3} K \bar{u}_1$ which justifies the above assumption. Therefore, to $O(\epsilon^{4/3})$, (23) becomes

$$(\bar{\rho}_2 + \bar{u}_2 + K\bar{u}_1 - M_\infty^2 \bar{u}_1^2)_{\bar{x}} + \bar{v}_{1\tilde{y}} = 0, \tag{29}$$

(24) gives

$$\left(\gamma_a M_\infty^2\left(\bar{\rho}_2 + 2\bar{u}_2 + \bar{u}_1^2(1 - 2M_\infty^2) + K\bar{u}_1\right) + \bar{p}_2\right)_{\bar{x}} + \gamma_a M_\infty^2 \bar{v}_{1\tilde{y}} = 0, \tag{30}$$

(26) gives

$$\bar{T}_2 = -(\gamma_a - 1)M_\infty^2\left(\bar{u}_2 + \frac{\bar{u}_1^2}{2}\right) + \bar{g}_1 K_\omega \frac{h_{fg}(T_\infty)}{C_{pa}T_\infty}, \tag{31}$$

and (27) gives

$$\bar{T}_2 = \bar{p}_2 - \bar{\rho}_2 - (\gamma_a - 1)M_\infty^4 \bar{u}_1^2 + \bar{g}_1 K_\omega \frac{\mu_a}{\mu_v}. \tag{32}$$

Equations (29)–(32) result, after some algebraic calculations, in

$$\left[K - (\gamma_a + 1)M_\infty^2 \bar{u}_1\right]\bar{u}_{1\bar{x}} + \bar{v}_{1\tilde{y}} = \bar{g}_{1\bar{x}} K_\omega\left(\frac{h_{fg}(T_\infty)}{C_{pa}T_\infty} - \frac{\mu_a}{\mu_v}\right). \tag{33}$$

Also, from (25) and (28) we can show that:

$$\bar{u}_{1\tilde{y}} - \bar{v}_{1\bar{x}} = 0. \tag{34}$$

The system of equations (33) and (34) is an extended formulation of the Kármán–Guderley system for a small-disturbance transonic flow of moist air. The system includes a heat source term in (33) which is related to the condensate mass fraction perturbation, $\bar{g}_1$. From (34), we find that the transonic flow of moist air is irrotational and, therefore, isentropic to the leading order, $O(\epsilon^{2/3})$, of the perturbations in the pressure, density, temperature, and axial velocity (see a similar result in Zierep 1969 and Schnerr & Mundinger 1993). We define a velocity perturbation potential, $\phi_1(\bar{x}, \tilde{y})$, related to the velocity perturbations: $\bar{u}_1 = \phi_{1\bar{x}}$ and $\bar{v}_1 = \phi_{1\tilde{y}}$. This satisfies an extended Kármán–Guderley equation:

$$\left[K - (\gamma_a + 1)M_\infty^2 \phi_{1\bar{x}}\right] \phi_{1\bar{x}\bar{x}} + \phi_{1\tilde{y}\tilde{y}} = \bar{g}_{1\bar{x}} K_\omega \left(\frac{h_{fg}(T_\infty)}{C_{pa} T_\infty} - \frac{\mu_a}{\mu_v} \right). \tag{35}$$

This is a non-homogeneous and nonlinear partial differential equation that can change its type depending on the local Mach number M where it can be shown that $M^2 - 1 = -\epsilon^{2/3}[K - (\gamma_a + 1)M_\infty^2 \phi_{1\bar{x}}]$. When locally the flow is subsonic, $M < 1$, the equation is elliptic and when the flow is supersonic, $M > 1$, the equation is hyperbolic. In the case of dry air $\bar{g}_1 = 0$ and (35) reduces to the classical transonic small-disturbance equation (Cole & Cook 1986). Moreover, (35) shows that in the flow regions of moist air with no condensation, where $\bar{g}_{1\bar{x}} = 0$, the solution is the same as that for dry air. Similar behaviour can be observed in the computations of Schnerr & Dohrmann (1990, figures 9 and 11, and 1994, figure 4); it can be seen that in the flow regions where condensation does not occur the solutions for the various cases with $\Phi_0 \neq 0$ coincide with the solution for the case with $\Phi_0 = 0$.

The boundary conditions (17) and far-field conditions (18) reduce in the leading orders to

$$\left.\begin{aligned} \phi_{1\tilde{y}}(\bar{x}, 0\pm) = F'_{u,l}(\bar{x}) \quad \text{for} \quad 0 \leqslant \bar{x} \leqslant 1, \quad \phi_{1\bar{x}}(1, 0^+) = \phi_{1\bar{x}}(1, 0^-), \\ \phi_{1\bar{x}}, \phi_{1\tilde{y}} \to 0 \quad \text{as } \bar{x} \to -\infty. \end{aligned}\right\} \tag{36}$$

We now analyse the condensation equations (A 1)–(A 4) and (11)–(16). The following non-dimensional parameters are defined:

$$\bar{p}_g(\bar{T}) = \frac{p_g(T)}{p_g(T_\infty)}, \quad \bar{\sigma}_\infty(\bar{T}) = \frac{\sigma_\infty(T)}{\sigma_\infty(T_\infty)}, \quad \bar{\rho}_l(\bar{T}) = \frac{\rho_l(T)}{\rho_l(T_\infty)}. \tag{37}$$

It can be shown from (A 4) that

$$\frac{\mathrm{d}r}{\mathrm{d}t} = u_c \frac{\mathrm{d}\bar{r}}{\mathrm{d}\bar{t}}, \quad \frac{\mathrm{d}\bar{r}}{\mathrm{d}\bar{t}} = \frac{\alpha(\bar{T})}{\sqrt{\bar{T}}} \left(\bar{p}(1 - \bar{g}) - K_{pg} \bar{p}_g(\bar{T}) \right). \tag{38}$$

Here $K_{pg} = (\mu_v/\mu_a) p_g(T_\infty)/(p_\infty \omega_\infty)$ is a similarity parameter relating the pressure of the upstream flow and initial specific humidity. It can also be shown from (A 1), (A 3), and the definitions of l_c and u_c that

$$\bar{J} = \omega_\infty \mathscr{J}, \quad \mathscr{J} = \sqrt{\frac{27}{32\pi^3}}\, n_c^{3/2} \frac{\bar{\rho}^2}{\bar{\rho}_l} \sqrt{\bar{\sigma}_\infty(\bar{T})} (1 - \bar{g})^2 \exp\left(-\frac{n_c \bar{\sigma}_\infty^3}{2\bar{T}^3 (\ln S)^2} \right). \tag{39}$$

Here, $n_c = (4\pi/3)\rho_{l\infty} l_c^3/m$ is the number of molecules in a characteristic droplet and

$m_c = (4\pi/3)\rho_{l\infty} l_c^3$ is its mass. The supersaturation ratio S in (39) is computed from (16):

$$\left.\begin{aligned} S &= \frac{p_v}{p_g(T)} = S_\infty \frac{\bar{p}(1-\bar{g}_1)}{\bar{p}_g(\bar{T})} + \cdots, \quad S_\infty = K_{pg}^{-1}, \\ p_v &= \frac{p_\infty \omega_\infty \bar{p}(1-\bar{g})}{\omega_\infty(1-\bar{g}) + (1-\omega_\infty)\mu_v/\mu_a}. \end{aligned}\right\} \tag{40}$$

When $S < 1$ we set $\mathscr{J} = 0$.

Note that $t_c = l_c/u_c$ is the characteristic time of the condensation process and $t_p = c/U_\infty$ is the characteristic time of the flow. We define $K_t = t_p/t_c = cu_c/l_c U_\infty$ as the ratio between the two time scales. When $K_t < 1$, the flow particles are convected along the airfoil with no condensation. However, when $K_t \gg 1$, the condensation time scale is much shorter than the convection time and condensation may take place around the airfoil. It can be shown from the definitions of l_c and u_c that

$$K_t = \sqrt{\frac{(\mu_a/\mu_v)^3}{8\pi\gamma_a}} \frac{p_\infty c\ \omega_\infty}{\sigma_\infty(T_\infty) M_\infty}. \tag{41}$$

This means that K_t is another similarity parameter of the condensation process which relates the airfoil chord, the pressure and Mach number of the upstream flow, and the initial specific humidity.

Substituting (20), (22), (38), (39), and (41) into (11)–(14) results in the relations among the leading-order terms of the condensation parameters:

$$\bar{g}_{1\bar{x}} = 4\pi K_t \left(\bar{Q}_{11} \frac{\mathrm{d}\bar{r}}{\mathrm{d}\bar{t}} + \tfrac{1}{3}\mathscr{J}\bar{r}_0^3 \right), \tag{42}$$

$$\bar{Q}_{11\bar{x}} = K_t \left(2\bar{Q}_{21} \frac{\mathrm{d}\bar{r}}{\mathrm{d}\bar{t}} + \mathscr{J}\bar{r}_0^2 \right), \tag{43}$$

$$\bar{Q}_{21\bar{x}} = K_t \left(\bar{Q}_{31} \frac{\mathrm{d}\bar{r}}{\mathrm{d}\bar{t}} + \mathscr{J}\bar{r}_0 \right), \tag{44}$$

$$\bar{Q}_{31\bar{x}} = K_t \mathscr{J}. \tag{45}$$

Here we set $\bar{r}_0 = r_0/l_c$. Since typically $r_0 = 1.3r^*$, $\bar{r}_0 \sim O(1)$. Note that when $K_t \gg 1$ it can be shown that the terms with $\bar{r}_0$ in (42)–(45) may be neglected.

Equations (42)–(45) do not involve the $\tilde{y}$-coordinate due to the transonic rescaling of the vertical coordinate. This set of equations together with (39) is a complicated system of first-order nonlinear and closed-coupled ordinary differential equations for the solution of the functions $\bar{g}_1$, $\bar{Q}_{11}$, $\bar{Q}_{21}$, and $\bar{Q}_{31}$. The far-field conditions:

$$\bar{g}_1 = \bar{Q}_{11} = \bar{Q}_{21} = \bar{Q}_{31} = 0 \quad \text{as} \quad \bar{x} \to -\infty \tag{46}$$

are used as initial values for the integration of these equations. The properties $\mathscr{J}$ and $\mathrm{d}\bar{r}/\mathrm{d}\bar{t}$ are calculated according to (38)–(40) in terms of the solution of (35) for $\phi_1(\bar{x}, \tilde{y})$. Notice that in computing these terms we use

$$\bar{T} = 1 - \epsilon^{2/3}(\gamma_a - 1)M_\infty^2 \phi_{1\bar{x}} + \epsilon^{4/3} \left(K_\omega \frac{h_{fg}(T_\infty)}{C_{pa} T_\infty} \right) \bar{g}_1 + \cdots \tag{47}$$

for higher accuracy of the computations. We include in (47) the leading-order effects of the changes in velocity ($O(\epsilon^{2/3})$ term) and in condensate mass fraction ($O(\epsilon^{4/3})$ term) on the temperature field.

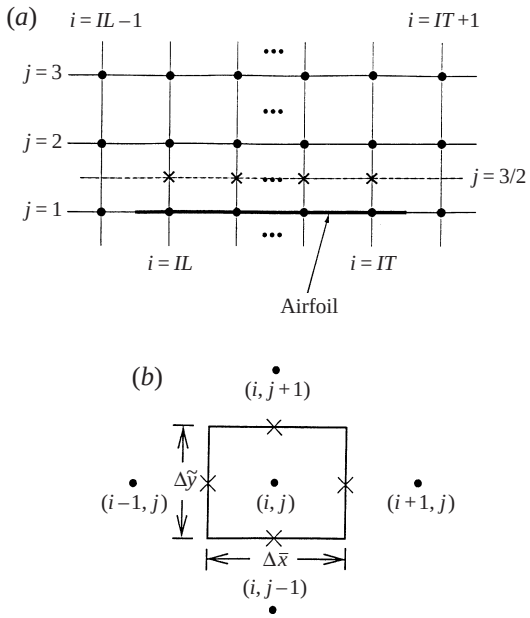

FIGURE 2. (*a*) The computational grid around an airfoil. (*b*) A control volume around a grid point.

The transonic small-disturbance theory for a flow of moist air around a thin airfoil results in an extended version of the Kármán–Guderley equation (35) for the solution of ϕ_1 coupled with a system of ordinary differential equations (42)–(45) for the solution of $\bar{g}_1$, with relations (38)–(40) for the condensation properties, and with boundary and far-field conditions (36) and (46). The problem involves the similarity parameters K, K_ω, $K_{pg}(=1/S_\infty)$, K_t, and n_c which is a function of the far-field temperature T_∞. The solution of the problem provides the pressure field $\bar{p} = p/p_\infty = 1 - \epsilon^{2/3}\gamma_a M_\infty^2 \phi_{1\bar{x}} + \cdots$ and the pressure coefficient $c_p = (p - p_\infty)/(\frac{1}{2}\rho_\infty U_\infty^2) = -2\epsilon^{2/3}\phi_{1x} + \cdots$. The temperature field is given by (47). The solution also provides the field of the condensate mass fraction $g = \epsilon^{4/3} K_\omega \bar{g}_1 + \cdots$ and the vapour pressure field $p_v = S_\infty p_g(T_\infty)\bar{p}(1 - \bar{g}_1) + \cdots$.

It is expected that increasing K_ω with fixed values of K and T_∞ creates a greater heat supply to the flow. This effect may be nonlinear and is demonstrated in the results of the computations presented in § 5. Also, it is expected that increasing K_t (by increasing the airfoil's chord or the free-stream pressure or decreasing the free-stream Mach number) increases the condensate mass fraction and, thereby, increases the amount of heat supply to the flow.

4. Numerical scheme

The transonic small-disturbance problem for moist air given by (35) and (42)–(45) may change its type according to the local flow conditions and, therefore, requires a type-sensitive difference scheme for a numerical solution. In the present approach we use the Murman & Cole (1971) technique for the solution of (35). According to this method, a test has to be devised to decide if a computational grid point is of elliptic type, hyperbolic type, or mixed type. The appropriate difference scheme is then used at that point at each step of the iterations.

For numerical consistency, a conservative form of (35) is used, i.e.

$$\left(K\phi_{1\bar{x}} - \tfrac{1}{2}(\gamma_a+1)M_\infty^2\phi_{1\bar{x}}^2\right)_{\bar{x}} + (\phi_{1\tilde{y}})_{\tilde{y}} = \bar{g}_{1\bar{x}}K_\omega\left(\frac{h_{fg}(T_\infty)}{C_{pa}T_\infty} - \frac{\mu_a}{\mu_v}\right). \tag{48}$$

The flow domain is divided into a uniform rectangular finite difference mesh with equal spacing $\Delta\bar{x}$ and $\Delta\tilde{y}$ and with grid points labelled by (i, j). The $j = 1$ line is assigned to the airfoil surface and the boundary condition of (36) is set on the line $j = \frac{3}{2}$ (see figure 2*a*). From the control volume diagram around a grid point (i, j) (see figure 2*b*), the finite difference equation at this point is

$$\begin{aligned}&\left(K\phi_{1\bar{x}} - \tfrac{1}{2}(\gamma_a+1)M_\infty^2\phi_{1\bar{x}}^2\right)_{i+1/2,j}\Delta\tilde{y} - \left(K\phi_{1\bar{x}} - \tfrac{1}{2}(\gamma_a+1)M_\infty^2\phi_{1\bar{x}}^2\right)_{i-1/2,j}\Delta\tilde{y}\\ &\quad+\{(\phi_{1\tilde{y}})_{i,j+1/2} - (\phi_{1\tilde{y}})_{i,j-1/2}\}\Delta\bar{x}\\ &= (\bar{g}_{1\bar{x}})_{i,j}K_\omega\left(\frac{h_{fg}(T_\infty)}{C_{pa}T_\infty} - \frac{\mu_a}{\mu_v}\right)\Delta\bar{x}\Delta\tilde{y}.\end{aligned} \tag{49}$$

Two stability factors:

$$\begin{aligned}(fuc)_{i,j} &= -K + \frac{\gamma_a+1}{2}M_\infty^2\,\frac{(\phi_1)_{i+1,j} - (\phi_1)_{i-1,j}}{\Delta\bar{x}},\\ (fub)_{i,j} &= -K + \frac{\gamma_a+1}{2}M_\infty^2\,\frac{(\phi_1)_{i,j} - (\phi_1)_{i-2,j}}{\Delta\bar{x}}\end{aligned}$$

are used to determine the type of the equation at a grid point according to the following criteria (see Murman & Cole 1971). A grid point is an elliptic (subsonic) point when $fuc_{i,j} < 0$ and $fub_{i,j} < 0$, a hyperbolic (supersonic) point when $fuc_{i,j} > 0$ and $fub_{i,j} > 0$, a sonic point when $fuc_{i,j} > 0$ and $fub_{i,j} < 0$, and a shock point when $fuc_{i,j} < 0$ and $fub_{i,j} > 0$. At each point, we use a special difference scheme for the $\bar{x}$-derivatives of both ϕ_1 and $\bar{g}_1$ to account for the physical propagation of information in the various regions of the flow.

When the equation at a grid point is elliptic, a central difference is used for the $\bar{x}$-derivatives:

$$\left.\begin{aligned}(\phi_{1\bar{x}})^{(C)}_{i+1/2,j} &= \frac{(\phi_1)_{i+1,j} - (\phi_1)_{i,j}}{\Delta\bar{x}}, \quad (\phi_{1\bar{x}})^{(C)}_{i-1/2,j} = \frac{(\phi_1)_{i,j} - (\phi_1)_{i-1,j}}{\Delta\bar{x}},\\ (\bar{g}_{1\bar{x}})^{(C)}_{i,j} &= \tfrac{(\bar{g}_1)_{i+1,j} - (\bar{g}_1)_{i-1,j}}{2\Delta\bar{x}}.\end{aligned}\right\} \tag{50}$$

When it is hyperbolic at a grid point, a backward difference is used for the $\bar{x}$-derivatives:

$$\left.\begin{aligned}(\phi_{1\bar{x}})^{(B)}_{i+1/2,j} &= \frac{(\phi_1)_{i,j} - (\phi_1)_{i-1,j}}{\Delta\bar{x}}, \quad (\phi_{1\bar{x}})^{(B)}_{i-1/2,j} = \frac{(\phi_1)_{i-1,j} - (\phi_1)_{i-2,j}}{\Delta\bar{x}},\\ (\bar{g}_{1\bar{x}})^{(B)}_{i,j} &= \frac{(\bar{g}_1)_{i,j} - (\bar{g}_1)_{i-2,j}}{2\Delta\bar{x}}.\end{aligned}\right\} \tag{51}$$

When a shock wave appears at (i, j), a mixed-type difference is used for the $\bar{x}$-derivatives:

$$\left.\begin{aligned}(\phi_{1\bar{x}})^{(S)}_{i+1/2,j} &= \frac{(\phi_1)_{i+1,j} - (\phi_1)_{i,j}}{\Delta\bar{x}}, \quad (\phi_{1\bar{x}})^{(S)}_{i-1/2,j} = \frac{(\phi_1)_{i-1,j} - (\phi_1)_{i-2,j}}{\Delta\bar{x}},\\ (\bar{g}_{1\bar{x}})^{(S)}_{i,j} &= \frac{(\bar{g}_1)_{i+1,j} - (\bar{g}_1)_{i,j} + (\bar{g}_1)_{i-1,j} - (\bar{g}_1)_{i-2,j}}{2\Delta\bar{x}}.\end{aligned}\right\} \tag{52}$$

When the point (i, j) is sonic, a central difference is used ahead of the point and a backward difference is used behind it. Therefore, at a sonic point $(\phi_{1\bar{x}})_{i-1/2,j} =$

$(\phi_{1\bar{x}})_{i+1/2,j}$ and $(\bar{g}_{1\bar{x}})_{i,j}$ is computed by a central difference. A central difference is used for the $\tilde{y}$-derivatives:

$$\left(\phi_{1\tilde{y}}\right)_{i,j+1/2} = \frac{(\phi_1)_{i,j+1} - (\phi_1)_{i,j}}{\Delta\tilde{y}}, \quad \left(\phi_{1\tilde{y}}\right)_{i,j-1/2} = \frac{(\phi_1)_{i,j} - (\phi_1)_{i,j-1}}{\Delta\tilde{y}}. \tag{53}$$

The boundary condition (36) along the airfoil chord is applied according to $(\phi_{1\tilde{y}})_{i,3/2} = (F'_{u,l})_i$ for every $IL \leqslant i \leqslant IT$ (here $i = IL$ is the grid line immediately after the leading edge and $i = IT$ is the grid line just before the trailing edge, see figure 2*a*). This condition is used when (49) is applied at grid points along the line $j = 2$. The far-field conditions in (36) are replaced by non-reflective conditions along the boundaries of the computational domain.

The above relations are applied to (49). An explicit method of iterations is used. The iterations usually start from initial disturbances given by the solution of a dry air flow around the airfoil. Equation (49) is numerically solved for a given distribution of the condensate mass fraction $\bar{g}_1(\bar{x}, \tilde{y})$. The solution of the perturbation potential ϕ_1 provides the fields of pressure $\bar{p}$ and temperature $\bar{T}$ that are needed in the computations of the condensation parameters.

In order to determine the field of $\bar{g}_1$, equations (42)–(45) are solved numerically by using the classical Simpson integration method for a first-order ordinary differential equation of the form $\bar{Q}_{\bar{x}} = f(\bar{x})$:

$$\bar{Q}_{i,j} = \bar{Q}_{i-1,j} + \frac{\Delta\bar{x}}{6}\left(f_{i-1,j} + 4f_{i-1/2,j} + f_{i,j}\right). \tag{54}$$

The far-field conditions (46) are used as the initial conditions for the integration process. The system of equations (42)–(45) is solved by iterations until the change in the maximum value of $\bar{g}_1$ in the flow field is less than 10^{-14}. In the solution of $\bar{g}_1$ we use the flow properties obtained from the previous iteration of (35).

Equations (35) and (42)–(45) are repeatedly solved until the solution converges at a certain iteration n, i.e. at any grid point (i, j): $\max_{i,j}\ (|\phi_{1ij,n} - \phi_{1ij,n-1}|) < 10^{-7}$ and $\max_{i,j}\ (|\bar{g}_{1ij,n} - \bar{g}_{1ij,n-1}|) < 10^{-14}$. Once convergence is found, the pressure coefficient along the airfoil's surfaces and the field of the condensate mass fraction can be described. The present numerical scheme is second-order in space, except across shock waves where it is first-order in space.

5. Numerical examples

The sensitivity of the numerical algorithm to grid refinement has been studied first. We concentrate on the case of a uniform flow with frozen free-stream Mach number $M_\infty = 0.8$, temperature $T_\infty = 259\,\mathrm{K}$, pressure $p_\infty = 65\,600\,\mathrm{Pa}$, and $S_\infty = 3.74$ ($\omega_\infty = 0.0074$) around a NACA0012 airfoil ($\epsilon = 0.12$) with chord $c = 0.1\,\mathrm{m}$ at zero angle of attack ($\Theta = 0$). These conditions correspond to the upstream flow conditions ahead of the airfoil with stagnation pressure $p_0 = 10^5\,\mathrm{Pa}$, temperature $T_0 = 293.15\,\mathrm{K}$, and relative humidity $\Phi_0 = 50\%$ which was studied by Schnerr & Dohrmann (1990). Also, for this case $K = 1.480$, $K_\omega = 0.123$, $K_{pg} = 0.266$, and $K_t = 263$. We concentrate here on the case where water vapour condenses to liquid only. A similar assumption was used in Schnerr & Dohrmann (1990).

Due to the symmetry of the problem around the $\bar{x}$-axis, only the upper flow domain is studied. We consider a computational domain of $3c$ (in the $\bar{x}$-direction) by $1.5c$ (in the $\tilde{y}$-direction), which is centred around the airfoil (with an upstream boundary $1c$ ahead of the leading edge and a downstream boundary $1c$ behind the trailing edge).

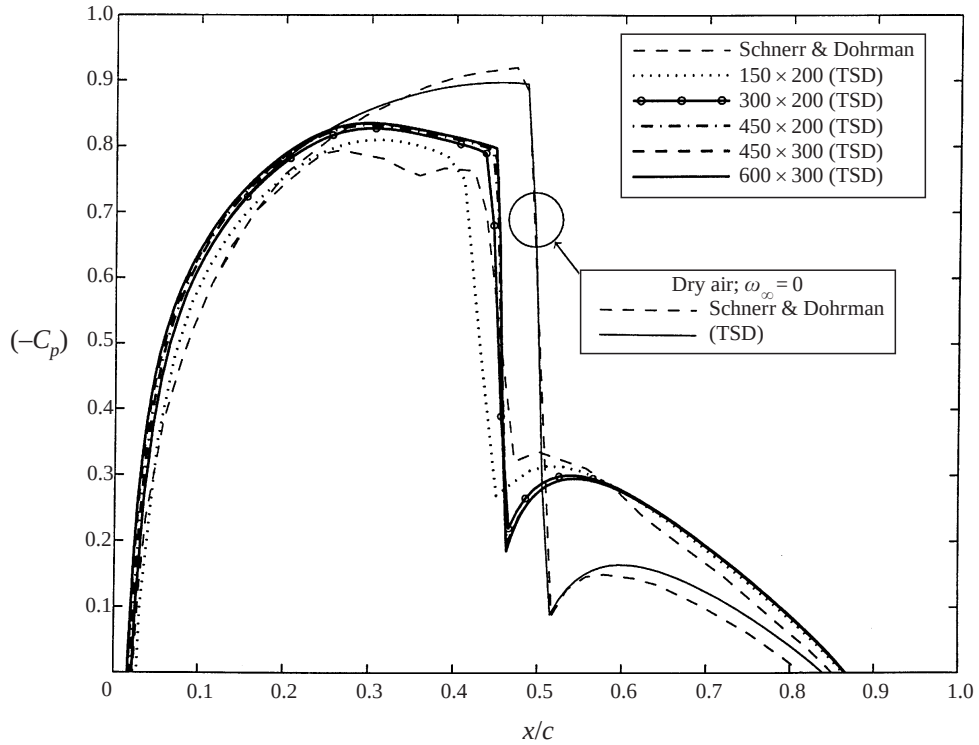

FIGURE 3. The distribution of pressure coefficient along a NACA0012 airfoil with $c = 0.1$ m at zero angle of attack, $M_\infty = 0.8$, $T_\infty = 259$ K, $p_\infty = 65\,600$ Pa, and $\omega_\infty = 0$ and 0.0074 according to TSD solutions using various meshes and the Euler solution of Schnerr & Dohrmann (1990).

Our experience, as well as previous numerical studies of the TSD problem for dry air (Cole & Cook 1986), shows that increasing the computational domain gives the same numerical solutions obtained by the domain $3c \times 1.5c$. Various meshes were used: 150 (in the $\bar{x}$-direction) by 200 (in the $\tilde{y}$-direction), 300 by 200, 450 by 200, 450 by 300, and 600 by 300. The resulting pressure coefficient along the airfoil's chord for the various meshes is shown in figure 3. The condensate mass fraction along the $\bar{x}$-axis is presented in figure 4. The change of vapour pressure with temperature along a streamline which runs close to the airfoil's surface is shown in the $p-T$ phase diagram in figure 5. We can see from figures 3 and 4 that the numerical solution converges as the mesh is refined in both the $\bar{x}$- and $\tilde{y}$-directions. A mesh of 450 by 300 may provide a sufficiently converged numerical solution in the present example. Such a mesh provides sufficiently converged results for other values of S_∞ in the range between 0 and 4.5.

Figures 3–5 also show the solution of Schnerr & Dohrmann (1990) for the same case. It can be seen that the solution according to the TSD model for moist air agrees within 5% of c_p with their solution. Specifically, notice that the smaller-scale parameters such as the condensate mass fraction and the complicated change of vapour pressure with temperature are almost the same as those predicted by Schnerr & Dohrmann (1990). Figure 6 presents contour lines of the condensate mass fraction field around the airfoil in this example. The $\bar{g}$-field is similar to the g/g_{max} contours in figure 12(c) of Schnerr & Dohrmann (1990). It can be seen from this figure that the condensation process starts at a certain point on the airfoil surface and that the condensate field develops in a narrow region around the airfoil and continues into the wake region.

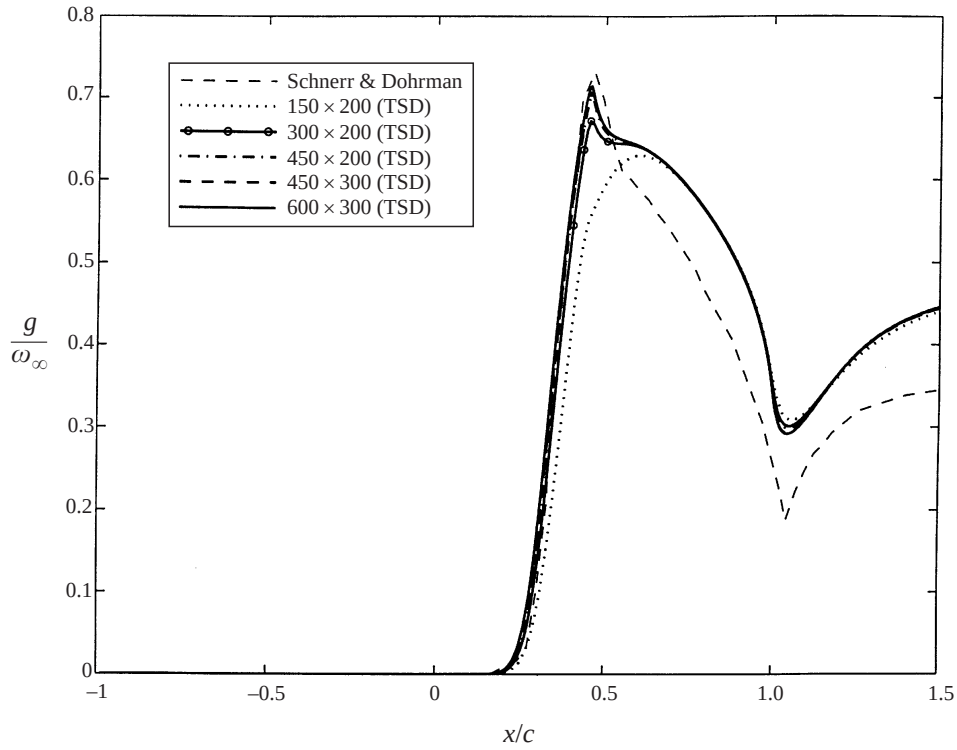

FIGURE 4. The distribution of condensate mass fraction along the airfoil according to TSD solutions using various meshes and the Euler solution of Schnerr & Dohrmann (1990).

Figures 3–6 together with the asymptotic formulae (28), (38), (39), (40), and (47) provide more insight into the details of the flow behaviour around the airfoil in this example. When the flow of moist air approaches the leading edge, it is forced to decelerate; $\bar{u}_1 < 0$ and the temperature and pressure increase, $\bar{T}_1 > 0$ and $\bar{p}_1 > 0$ (or $c_p > 0$). As a result, the ratio $\bar{p}_g$ increases above 1, the supersaturation ratio S decreases below S_∞, $\mathcal{J}$ is exponentially small, and no condensation occurs. When the flow expands around the leading edge and accelerates to speeds above U_∞, we have $\bar{u}_1 > 0$ and both the temperature and pressure decrease, $\bar{T}_1 < 0$ and $\bar{p}_1 < 0$ (or $c_p < 0$). As a result, the vapour pressure decreases, the ratio $\bar{p}_g$ also decreases significantly, and S increases. Only when the flow further accelerates to supersonic speeds and the temperature decreases below a critical value, does the supersaturation ratio S increase enough to make $\mathcal{J}$ sufficiently large. A significant condensation occurs over a short distance of about 5% of the airfoil's chord. The condensate mass fraction increases from zero to around 0.7 (about 70% of water vapour in the particles flowing near the airfoil surface condenses, see figure 4). The formation of condensate reduces the vapour pressure significantly as well as increases the temperature (see (40), (47), and figure 5). This causes the flow to decelerate and the pressure to increase compared to the dry air case (see (28) and figure 3). Therefore, the shock wave in the flow becomes less strong and shifts to an upstream position. Behind the shock wave, the flow decelerates back to subsonic speeds, the pressure and temperature increase, S becomes less than 1, and $\mathcal{J} = 0$. This means that behind the shock wave the condensation rate is negative and evaporation occurs (see (38) and figures 4 and 5). The local flow acceleration behind the shock wave is similar to that in the dry air

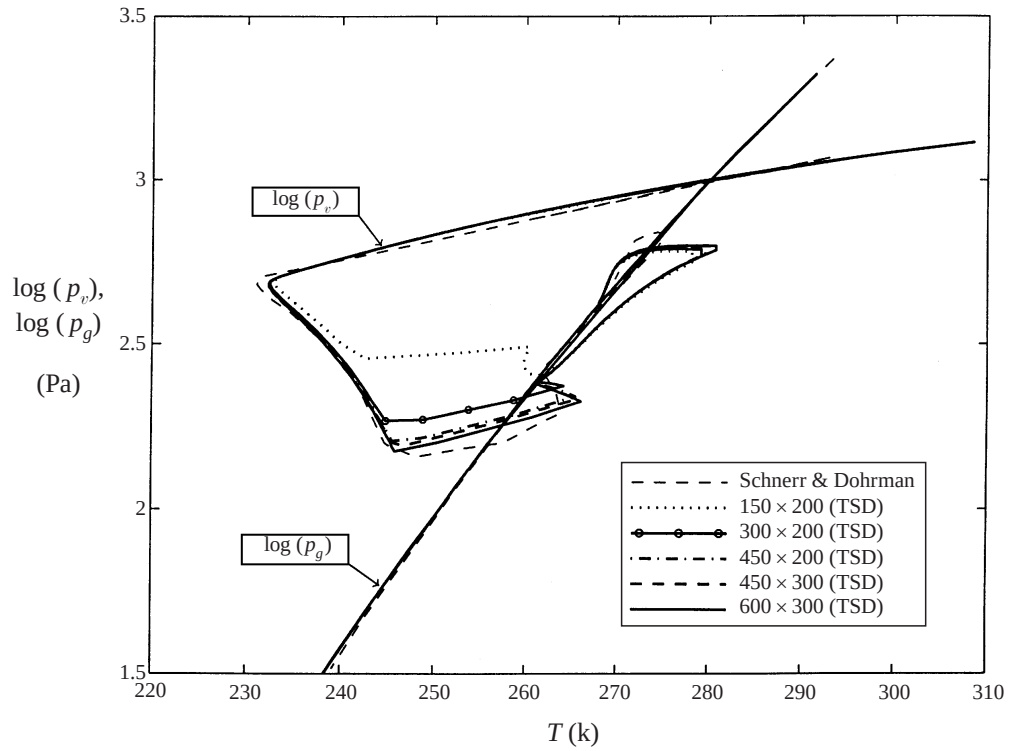

FIGURE 5. The change of the vapour pressure along a stream line that runs close to the airfoil in a p–T phase diagram according to TSD solutions using various meshes and the Euler solution of Schnerr & Dohrmann (1990).

case, known as the Oswatitsch–Zierep singularity (Oswatitsch & Zierep 1960). As the flow approaches the trailing edge, it decelerates, the pressure and temperature increase, and the evaporation of condensate mass continues (see figure 4). Behind the trailing edge, the flow accelerates to a uniform speed and the pressure and temperature decrease. Since S increases above 1 and there are droplets in the flow, the condensation process continues behind the airfoil. In the present example, the condensation process stabilizes in the far-wake region on $S = 1$ and $\bar{g} \sim 0.45$.

Figure 7 shows the distribution of the pressure coefficient along a NACA0012 airfoil for a flow with the same far-field conditions as listed above except $S_\infty = 4.49$ (or $\omega_\infty = 0.0088$). These conditions correspond to the upstream flow conditions ahead of the airfoil with stagnation pressure $p_0 = 10^5$ Pa, temperature $T_0 = 293.15$ K, and relative humidity $\Phi_0 = 60\%$ which was also studied by Schnerr & Dohrmann (1990). For this case $K = 1.480$, $K_\omega = 0.149$, $K_{pg} = 0.223$ and $K_t = 319$. The TSD solution has been computed in a $3c$ by $1.5c$ domain with a uniform mesh of 450 by 300. Again, the TSD solution shows agreement with the results of Schnerr & Dohrmann (1990) for this case. Specifically, in the present case we are able to resolve the weak condensation compression wave that occurs in the range $0.23 < \bar{x} < 0.35$ as well as the regular shock wave at $\bar{x} = 0.5$.

Figures 8 summarizes the results of computations according to the TSD model for moist air at various values of the initial specific humidity in the range $0 \leqslant \omega_\infty \leqslant 0.0088$. This corresponds to $0\% \leqslant \Phi_0 \leqslant 60\%$ in the computations of Schnerr & Dohrmann (1990). In all the cases the other upstream properties are the same as listed

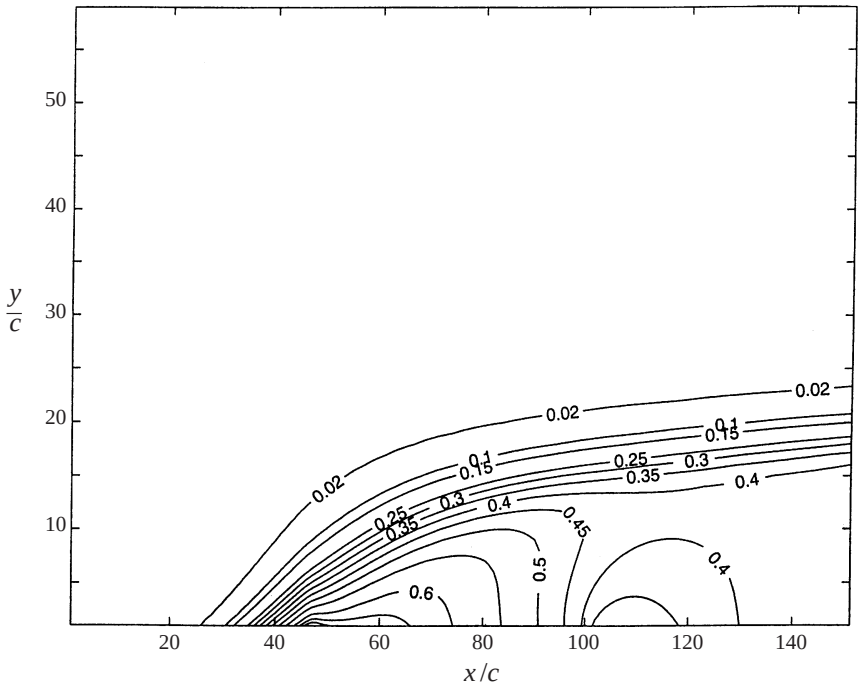

FIGURE 6. The field of condensate mass fraction around the airfoil according to the TSD solution.

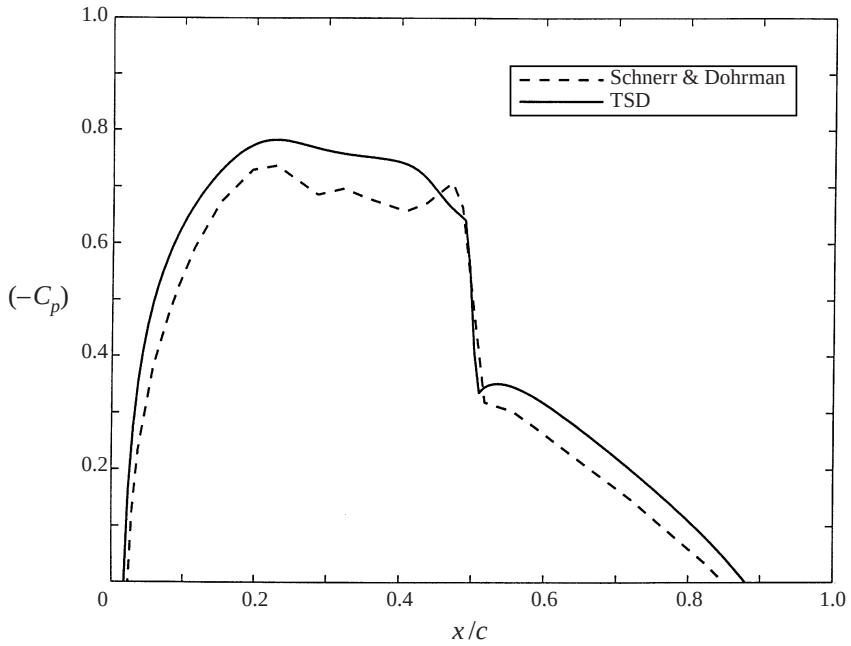

FIGURE 7. The distribution of pressure coefficient along a NACA0012 airfoil with $c = 0.1\,\text{m}$ at zero angle of attack, $M_\infty = 0.8$, $T_\infty = 259\,\text{K}$, $p_\infty = 65\,600\,\text{Pa}$, and $\omega_\infty = 0.0088$ according to TSD solution and the Euler solution of Schnerr & Dohrmann (1990).

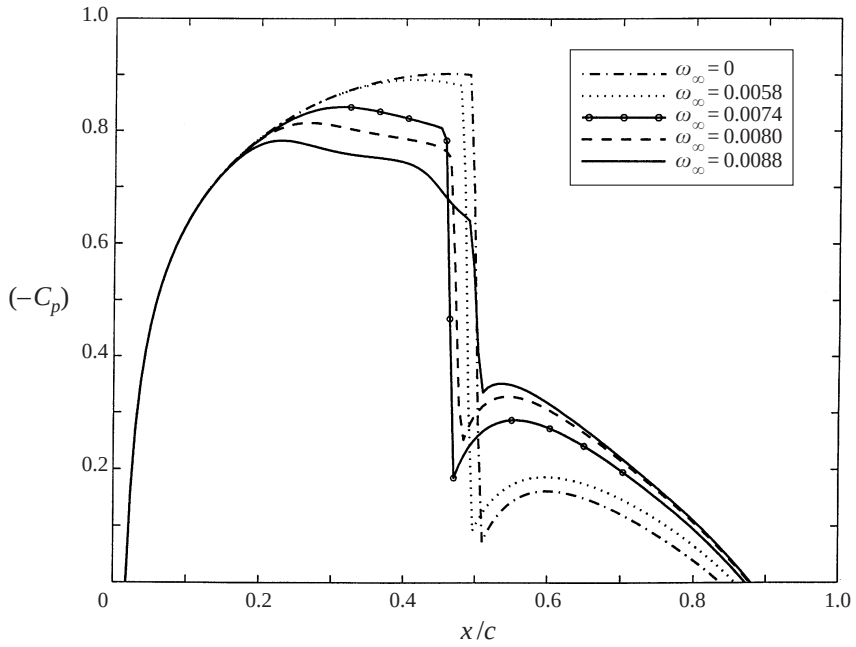

FIGURE 8. The distribution of pressure coefficient along a NACA0012 airfoil with $c = 0.1$ m at zero angle of attack, $M_\infty = 0.8$, $T_\infty = 259$ K, $p_\infty = 65\,600$ Pa, and various values of ω_∞.

above. It can be seen that as ω_∞ increases, the range of the effect of condensation also increases over the airfoil. The resulting increase of pressure and reduction of strength of the regular shock wave are significant. Moreover, figure 8 shows an upstream shift in the shock position when ω_∞ is increased up to 0.0074 and a downstream shift in the shock wave position when ω_∞ is further increased above 0.0074. The variation of the shock wave position is summarized in figure 9. Again, the results from the TSD model show a good agreement with the computations of Schnerr & Dohrmann (1990).

The change of the shock position around $\omega_\infty = 0.0074$ may be explained by the change in the nature of the condensation field when ω_∞ is increased. In the examples studied here, when $0 < \omega_\infty < 0.0074$ the condensation field is continuous and its onset point moves upstream along the airfoil's surface as ω_∞ is increased. This phenomenon occurs because the critical temperature for the onset of a significant condensation increases with ω_∞ (see figure 10). The increase of the initial specific humidity creates more heat of condensation which decelerates the flow ahead of the regular shock wave. This causes the shock wave to reduce its strength and to shift upstream. However, when $\omega_\infty > 0.0074$, the amount of heat supplied by condensation is more than the flow can absorb and, therefore, a weak condensation compression wave is formed over several percent of the airfoil's chord in front of the regular shock wave. The condensation compression wave causes the flow to decelerate and the pressure and temperature behind it to increase a little. As a result, the regular shock wave is pushed downstream compared to its position when $\omega_\infty = 0.0074$. When ω_∞ is increased much above 0.0074, the condensation compression wave becomes more strong and noticeable (see the schematics in figure 2 in Schnerr & Dohrmann 1994 for a NACA0012 airfoil).

Figure 10 shows the TSD results for the vapour pressure as function of temperature

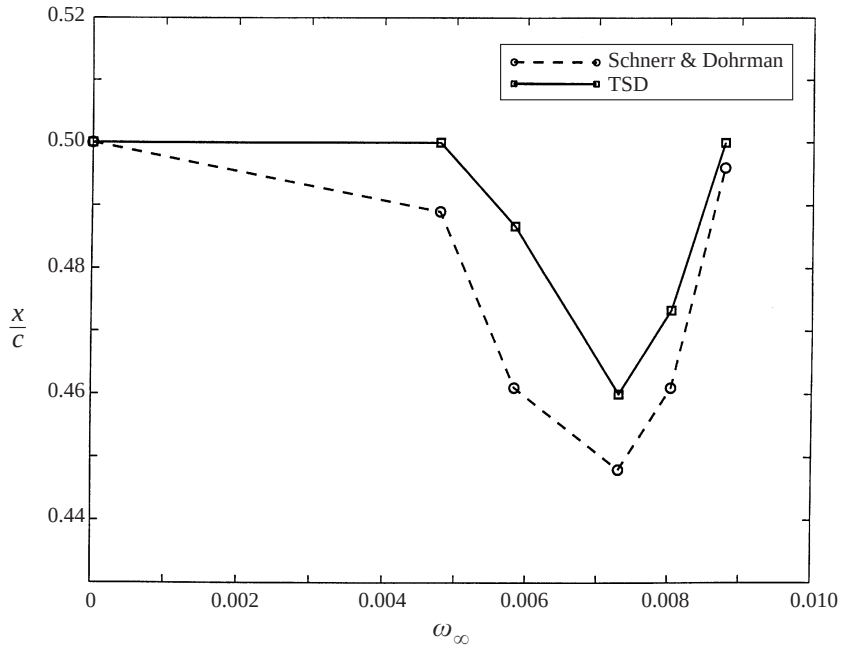

FIGURE 9. The shift of shock wave position according to TSD solution and the Euler solution of Schnerr & Dohrmann (1990).

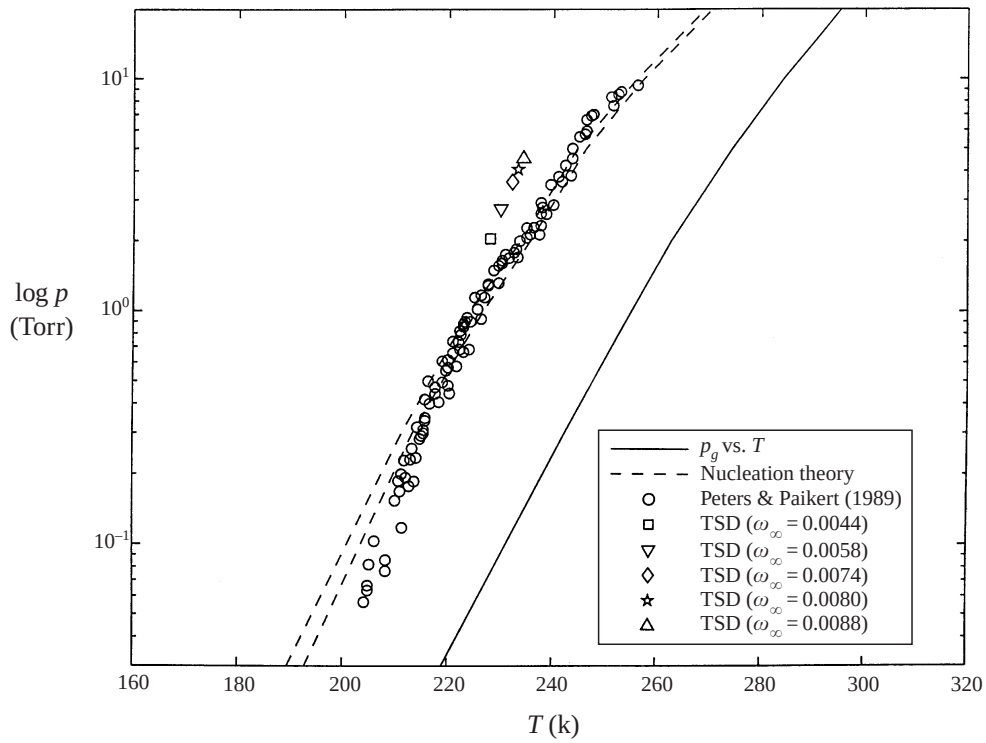

FIGURE 10. Comparison of TSD results for the onset of non-equilibrium condensation with classical nucleation theory and experimental data in a p–T phase diagram.

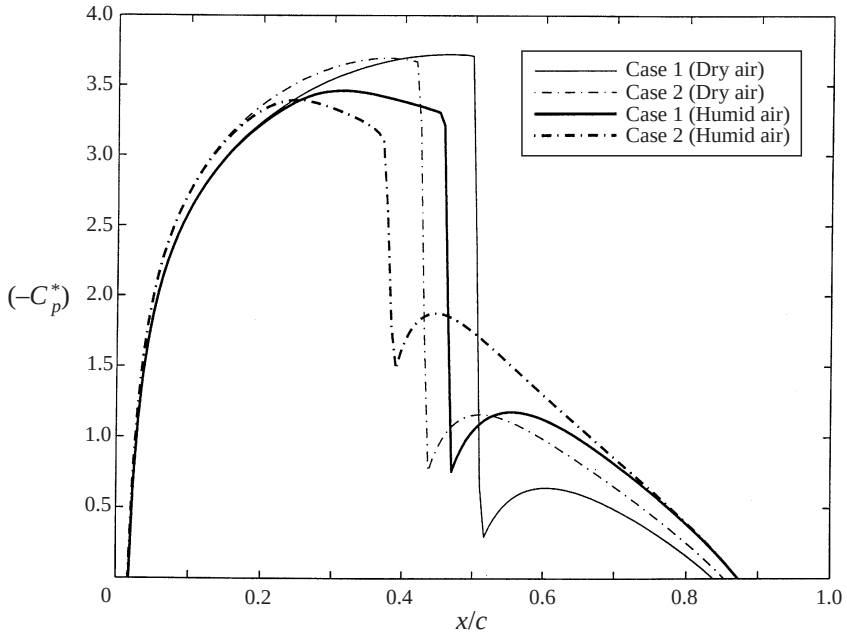

FIGURE 11. The distribution of the scaled pressure coefficient along NACA airfoils for the two self-similar cases.

at the onset of condensation in each of the flows in figure 8. The onset of condensation in the present computations is defined as the point on the airfoil surface where the temperature of moist air reaches a minimum (critical) value. Also shown in this figure for comparison are the experimental results of Peters & Paikert (1989) for the onset conditions of condensation of water vapour in argon as measured in shock tube experiments and the curve according to the classical nucleation theory. It can be seen that the present results agree with the previously published empirical similarity law for the onset of condensation.

The present model gives the similarity parameters which govern the transonic flow of humid air around an airfoil. These parameters are used here to provide another set of flow conditions around a NACA airfoil at zero angle of attack. The behaviour of this new flow is expected to be sufficiently close to the flow around a NACA0012 at $M_\infty = 0.8$ and $\omega_\infty = 0.0074$ which was described above in figures 3–6 (case 1). In this second case, we choose $\epsilon = 0.15$ and $T_\infty = 259.0\,\mathrm{K}$. Keeping the same values of $K = 1.480$, $K_\omega = 0.123$, $K_{pg} = 0.266$, $K_t = 263$, we find that in the second case the chord $c = 0.095\,\mathrm{m}$, the free-stream frozen Mach number $M_\infty = 0.763$, the pressure $p_\infty = 49\,000\,\mathrm{Pa}$, and the initial specific humidity $\omega_\infty = 0.0098$. Figures 11–13 show the results of the TSD computations for the two cases. It can be seen that the behaviour of the scaled pressure coefficient $c_p^* = c_p/\epsilon^{2/3}$ vs. $\bar{x}$, g/ω_∞ vs. $\bar{x}$, and p_v vs. T are close to each other. The small deviation between the solutions is related to the difference in shock wave positions of the dry air cases (figure 11). These may appear as a result of the incomplete similarity in the TSD equation (35) related to the term which includes M_∞. Also, the small differences in the p–T diagram may be related to the second-order term in the temperature equation (47). These results demonstrate the most important aspect of the present asymptotic approach. The similarity parameters

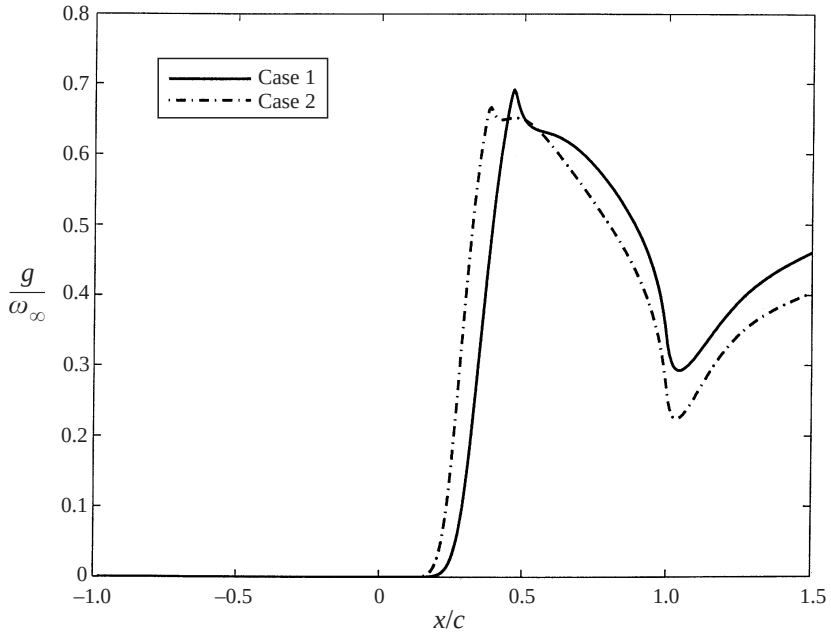

FIGURE 12. The distribution of the condensate mass fraction along NACA airfoils for the two self-similar cases.

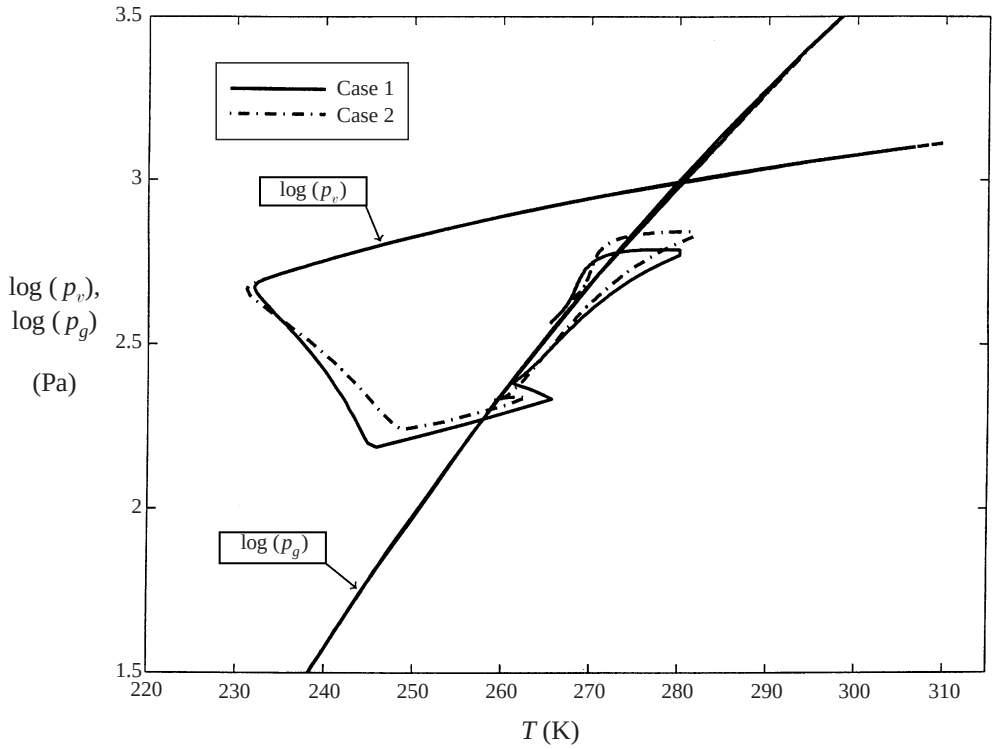

FIGURE 13. The change of the vapour pressure along a stream line that runs close to the airfoil in a p–T phase diagram for the two self-similar cases.

provide various flow cases with different flow properties which have a sufficiently close behaviour. Such cases cannot be predicted from numerical simulations or experiments only.

6. Conclusions

The steady transonic flow of moist air with non-equilibrium and homogeneous condensation around a thin airfoil can be described by a small-disturbance model. The model explores the nonlinear interactions among the near-sonic speed of the flow, the small thickness ratio and angle of attack of the airfoil, and the small amount of water vapour in the air. The flow field is governed by a non-homogeneous (extended) TSD equation coupled with a set of four ordinary differential equations for the calculation of the condensate (or sublimate) mass fraction. The asymptotic analysis gives the similarity parameters that govern the flow problem. These are the classical transonic parameter K which defines how close the free-stream speed is to the sonic speed, the humidity parameter K_ω which defines the amount of water vapour in the air, the supersaturation parameter $S_\infty = 1/K_{pg}$ which defines the ratio of the free-stream vapour pressure to the saturation pressure, the parameter K_t which defines the ratio of the convection time of the flow to the characteristic time of condensation, and the number of molecules in a characteristic droplet, n_c, which is a function of the free-stream temperature.

The Murman & Cole (1971) method and Simpson's rule of integration are combined into an iterative scheme which can be used to solve numerically the model equations. The results of the present computations show good quantitative agreement with available numerical simulations of Schnerr & Dohrmann (1990). The small differences between the solutions can be explained by the inherent inaccuracy of the small-disturbance theory near the stagnation regions and near shock waves. The model equations and results are also used to study the effects of heat supply by condensation on the flow field structure around an airfoil and the aerodynamic performance of the airfoil.

The present model is limited to the study of steady, inviscid, transonic flows of moist air around thin airfoils with non-equilibrium and homogeneous condensation. Previous studies of Laval nozzle flows show that there exists a limit for the amount of heat addition in steady transonic flows. Above this limit, the flow becomes unstable with self-excited periodic oscillations and complex dynamics. Zierep (1969) proposed an estimation for the critical heat input above which no steady-state solutions may exist. However, the estimation of such a limit case for an unbounded flow domain and the mechanism of loss of stability are still an open problem to investigate. Our experience also shows difficulties in finding steady-state solutions at high levels of humidity in the air. Extending the present model to study unsteady flows may provide a framework to tackle this complicated problem. Moreover, the effect of small viscosity on the flow dynamics and on the condensation behaviour are not known yet and present an additional difficulty. Specifically the nature of boundary layers of moist air should be investigated in more detail. The present model may provide the external flow conditions for the boundary layer flow. Finally, the model assumptions for the vapour content are only valid for experiments in transonic wind tunnels. In transonic atmospheric flight, supersaturated moist air with $S_\infty > 1$ is impossible (S_∞ must be less than or equal 1). Also, the related condensation dynamics is quite different. As mentioned above, transonic atmospheric flows are characterized by near-equilibrium and heterogeneous condensation process. Extending the present model to study the

aerodynamic behaviour of airfoils in such flows is also an interesting problem with applications in the design of airplanes, helicopters, and other flying vehicles.

Appendix A. Review of the theory of non-equilibrium and homogeneous condensation

Based on experimental data of the condensation of water vapour in cloud chambers and air nozzles, Wegener & Mack (1958) and Hill (1966) listed basic assumptions which describe the non-equilibrium and homogeneous condensation process. These can be summarized as follows: (*a*) the condensate mass in a fluid particle is often very small and the mass of each particle, composed of the flowing gaseous mixture, can be considered unchangeable during the process; (*b*) the liquid (or solid) condensate mass is uniformly distributed throughout the gaseous components of the fluid particle and has the same speed and temperature as the gaseous components of the particle; (*c*) the main effect of condensation is the release of heat of condensation during the nucleation of droplets in a particle to the gaseous components in a particle; (*d*) the surface tension of a droplet may be independent of curvature of the droplet surface and the interaction between droplets is negligible; (*e*) the critical-sized nucleus for a droplet that starts to grow is typically less than 1000 Å and much less than the mean free path. Even the size of the growing droplet, after travelling a long distance with a flow, is generally still less than the mean free path. Therefore, the motion of the droplets can be ignored in the estimation of the fluxes of mass and energy to and from the droplet surface. These may be computed according to the kinetic theory only. Finally, (*f*) the condensation is observed only at supersonic Mach numbers and takes place at high values of the supersaturation ratio, $S \sim 50$, or at even much greater values.

Based on these assumptions Volmer (1939), Zeldovich (1942), and Frenkel (1946) suggested a theory of the non-equilibrium and homogeneous condensation of water vapour in moist air. Once a critical nucleus is formed, its further growth is determined by a droplet nucleation law (see also Wegener & Mack 1958 and Hill 1966). They derived a law which describes the nucleation rate of the number of droplets per unit time and volume, J, in terms of the temperature, T, the Boltzmann constant, k, a nucleation factor, $\mathscr{K}$, and the critical work, W^*, which is required to produce one stable spherical droplet of critical size reversibly and isothermally. The nucleation factor, $\mathscr{K}$, depends on the mass per molecule of water, m, the surface tension of a plane surface, $\sigma_\infty(T)$, the vapour density, ρ_v, and the liquid density, ρ_l. The relations are given by

$$J = \mathscr{K} \exp\left(\frac{-W^*}{kT}\right), \quad \mathscr{K} = \sqrt{\frac{2\sigma_\infty(T)}{\pi}}\, m^{-3/2}\, \frac{\rho_v^2}{\rho_l}. \tag{A 1}$$

Notice that typically $\mathscr{K}$ has very large values, of the order of $10^{33}\,\mathrm{m^{-3}\,s^{-1}}$, since $m = \mu_v/N_A \sim 3 \times 10^{-26}\,\mathrm{kg}$ (here $\mu_v = 18.02\,\mathrm{kg\,kmole^{-1}}$ is the molecular weight of water, $N_A = 6.0225 \times 10^{26}$ molecules per kmole is Avogadro number, and the empirical relations of Schnerr & Dohrmann (1990) for $\sigma_\infty(T)$ in $\mathrm{N\,m^{-1}}$ are used). The critical work W^* was computed from the difference between the work $W_1 = 4\pi r^{*2}\sigma_\infty(T)$ done against the surface tension to increase the surface area of a spherical droplet from zero to a certain value, and the work $W_2 = (4\pi/3)(p_l - p_g)r^{*3}$ expended in the volume growth of the droplet. The work W_2 is driven by the difference between the pressure inside the droplet, p_l, and the surrounding saturated vapour pressure $p_v = p_g(T)$. Here r^* is the critical radius of the droplet. From the balance of stress on the droplet

surface we have $p_l - p_g = 2\sigma_\infty(T)/r^*$. Therefore, $W^* = W_1 - W_2 = (4\pi/3)r^{*2}\sigma_\infty(T)$. Using the Thomson–Gibbs equation for the vapour pressure of a critical droplet,

$$r^* = \frac{2\sigma_\infty(T)}{\rho_l R_v T \ln(S)} \tag{A 2}$$

(here R_v is the specific gas constant of water vapour) it was found that W^* is a function of the supersaturation ratio S and the temperature T, i.e.

$$W^* = \frac{16}{3}\pi \left(\frac{m}{\rho_l \ln(S)\, kT}\right)^2 \sigma_\infty^3(T). \tag{A 3}$$

Wegener & Mack (1958), Wegener & Pouring (1964), and Hill (1966) proposed that the rate at which the droplet grows is the difference between the condensation and evaporation rates. When the temperature of the water vapour and of the liquid droplet in a fluid particle are the same, this rate may be estimated by Hertz–Knudsen model:

$$\frac{\mathrm{d}r}{\mathrm{d}t} = \frac{\alpha(T)}{\rho_l} \frac{p_v - p_g(T)}{\sqrt{2\pi R_v T}}, \tag{A 4}$$

where $\alpha(T)$ is a condensation coefficient which depends on temperature and represents the proportion of molecules impinging on the droplet surface that stick to it. Notice that when $p_v > p_g(T)$ (or $S > 1$), $\mathrm{d}r/\mathrm{d}t > 0$ and the droplet grows. However, when $p_v < p_g(T)$ (or $0 < S < 1$), $\mathrm{d}r/\mathrm{d}t < 0$ and the droplet tends to evaporate and collapse.

Wegener & Mack (1958) and Hill (1966) also defined the condensate mass fraction g as the ratio of condensate mass to total mass of water vapour, condensate, and dry air. The parameter $g\,(> 0)$ is related with the amount of heat transfer to the fluid and affects the compressible fluid dynamics of moist air. Based on the nucleation rate equation for J and the droplet growth rate $\mathrm{d}r/\mathrm{d}t$, Hill (1966) developed an integro-differential model equation for computing the rate of change of g along a path line due to nucleation up to a certain position. This rate is composed of the nucleation rate at the initial droplet radius and the accumulation of growing spherical droplets in a fluid particle as it moves along a path line from far upstream, i.e.

$$\frac{\mathrm{d}g}{\mathrm{d}x} = \frac{4\pi\rho_l}{\dot{m}} \left[\int_{x_0}^{x} \left(r_0 + \int_{x_1}^{x} \frac{1}{u}\frac{\mathrm{d}r}{\mathrm{d}t}\,\mathrm{d}x_2\right)^2 J(x_1)A(x_1)\frac{1}{u}\frac{\mathrm{d}r}{\mathrm{d}t}\,\mathrm{d}x_1\right] + \frac{4\pi\rho_l r_0^3}{3\dot{m}} J(x)A(x). \tag{A 5}$$

Here r_0 is the initial radius of a nucleus, x_0 is the position of the initial nucleus, and $A(x)$ is the surface area of a spherical droplet at a position x along the path line of a fluid particle. Also, u is the local flow speed and $\dot{m}$ is the total flow rate of the gaseous components through the surface area $A(x)$, $\dot{m} = \rho u A$. The rate $\mathrm{d}/\mathrm{d}x = (1/u)\mathrm{d}/\mathrm{d}t$ where $\mathrm{d}/\mathrm{d}t$ is the substantial derivative.

Appendix B. Convenient formulae used in the analysis

Saturation vapour pressure of water $p_g(T)$ in mbar with T in (°C) is (Pruppacher & Klett 1980):

$$p_g(T) = a_0 + T\,(a_1 + T\,\{a_2 + T\,(a_3 + T\,[a_4 + T\,(a_5 + a_6\,T)])\})$$

for water liquid	for water ice
$a_0 = 6.107799961$	$a_0 = 6.109177956$
$a_1 = 4.436518521 \times 10^{-1}$	$a_1 = 5.034698970 \times 10^{-1}$
$a_2 = 1.428945805 \times 10^{-2}$	$a_2 = 1.886013408 \times 10^{-2}$
$a_3 = 2.650648471 \times 10^{-4}$	$a_3 = 4.176223716 \times 10^{-4}$
$a_4 = 3.031240396 \times 10^{-6}$	$a_4 = 5.824720280 \times 10^{-6}$
$a_5 = 2.034080948 \times 10^{-8}$	$a_5 = 4.838803174 \times 10^{-8}$
$a_6 = 6.136820929 \times 10^{-11}$	$a_6 = 1.838826904 \times 10^{-11}$.

Saturated liquid density ρ_l in ($\mathrm{kg\,m^{-3}}$) is (Pruppacher & Klett 1980):

$$T > 0(^\circ\mathrm{C}):\ \rho_l = (999.8396 + 18.224944\,T - 7.922210 \times 10^{-3}\,T^2 - 55.44846 \times 10^{-6}\,T^3 + 149.7562 \times 10^{-9}\,T^4 - 393.2952 \times 10^{-12}\,T^5)/(1 + 18.159725 \times 10^{-3}\,T),$$

$$T < 0(^\circ\mathrm{C}):\ \rho_l = (0.99984 + 0.86 \times 10^{-4}\,T - 0.108 \times 10^{-4}\,T^2) \times 1000.$$

Surface tension σ_∞ in ($\mathrm{N\,m^{-1}}$) is (Schnerr & Dohrmann 1990):

$$T > 273.15\,\mathrm{K}:\ \sigma_\infty(T) = (75.75 + 0.151(273.15 - T)) \times 10^{-3},$$
$$T < 273.15\,\mathrm{K}:\ \sigma_\infty(T) = (96.0 - 0.29(273.15 - T)) \times 10^{-3}.$$

Condensation coefficient α is (Schnerr & Dohrmann 1990):

$$T > 270\,\mathrm{K}:\ \alpha(T) = 0.5,$$
$$230 < T < 270\,\mathrm{K}:\ \alpha(T) = 1 - 0.0125(T - 230),$$
$$T < 230\,\mathrm{K}:\ \alpha(T) = 1.0.$$

Specific latent heat $h_{fg}(T)$ in ($\mathrm{cal\,g^{-1}}$) is (Pruppacher & Klett 1980):

$$h_{fg}(T) = 597.3 \times (273.15/T)^b, \quad b = 0.167 + 3.67 \times 10^{-4} \times T.$$

REFERENCES

Abraham, F. F. 1974 *Homogeneous Nucleation Theory*. Academic.

Campbell, J. F., Chambers, J. R. & Rumsey, C. L. 1989 Observation of airplane flow fields by natural condensation. *J. Aircraft* **26**, 593–604.

Cole, J. D. & Cook, L. P. 1986 *Transonic Aerodynamics*. North-Holland.

Frenkel, J. 1946 *Kinetic Theory of Liquids*. Dover.

Hall, R. M. 1979 Onset of condensation effects with an NACA 0012-64 airfoil tested in the Langley 0.3-meter transonic cryogenic wind tunnel technology. *NASA TP* 1385.

Head, R. 1949 Investigation in spontaneous condensation phenomena. PhD thesis, California Inst. of Technology.

Hill, P. G. 1966 Condensation of water vapour during supersonic expansion in nozzles. *J. Fluid Mech.* **25**, 593–620.

Jordan, F. L. 1972 Investigation at near-sonic speed of some effects of humidity on the longitudinal aerodynamic characteristics of a NASA supercritical wing research airplane model. *NASA TM* X-2618.

Moran, M. J. & Shapiro, H. N. 1992 *Fundamentals of Engineering Thermodynamics*, 3rd Edn. John Wiley & Sons.

Murman, E. M. & Cole, J. D. 1971 Calculation of plane study transonic flows. *AIAA J.* **9**, 114–121.

Murray, R. S. 1968 *Mathematical Handbook of Formulas and Tables*. McGraw-Hill.

Oswatitsch, K. & Zierep, J. 1960 Das problem des senkrechten stoβes an einer gekrümmten Wand. *Z. Angew. Math. Mech.* **40**, 143–144.

Peters, F. 1983 A new method to measure homogeneous nucleation rates in shock tubes. *Exps. Fluids* **1**, 143–148.

PETERS, F. & PAIKERT, B. 1989 Nucleation and growth rates of homogeneously condensing water vapour in argon from shock tube experiments. *Exps. Fluids* **7**, 521–530.

PRUPPACHER, H. R. & KLETT, J. D. 1980 *Microphysics of Clouds and Precipitation.* D. Reidel.

SCHMIDT, B. 1966 Schallnahe profilumströmungen mit kondensation. *Acta Mechanica* **2**, 194–208.

SCHNERR, G. H. & DOHRMANN, U. 1990 Transonic flow around airfoils with relaxation and energy supply by homogeneous condensation. *AIAA J.* **28**, 1187–1193.

SCHNERR, G. H. & DOHRMANN, U. 1994 Drag and lift nonadiabatic transonic flow. *AIAA J.* **32**, 101–107.

SCHNERR, G. H. & MUNDINGER, G. 1993 Similarity, drag and lift in transonic flow with given internal heat addition. *Eur. J. Mech.* B/*Fluids* **12**, 597–612.

VOLMER, M. 1939 *Kinetik der Phasenbildung*. Steinopff-Verlag, Leipzig.

WEGENER, P. P. 1969 Gas dynamics of expansion flows with condensation, and homogeneous nucleation of water vapour. In *Nonequilibrium Flows,* part 1, chap. 4. Marcel Dekker.

WEGENER, P. P. 1975 Nonequilibrium flow with condensation. *Acta Mechanica* **21**, 65–91.

WEGENER, P. P. 1987 Nucleation of nitrogen: experiment and theory. *J. Phys. Chem.* **91**, 2479–2481.

WEGENER, P. P. & MACK, L. M. 1958 Condensation in supersonic and hypersonic wind tunnels. *Adv. Appl. Mech.* **5**, 307–447.

WEGENER, P. P. & POURING, A. A. 1964 Experiments on condensation of water vapour by homogeneous nucleation in nozzles. *Phys. Fluids* **7**, 352–361.

ZELDOVICH, Y. B. 1942 Theory of the formation of a new phase cavitation. *J. Expl Theor. Phys. (USSR)* **12**, 525.

ZETTLEMOYER, A. C. 1969 *Nucleation.* Marcel Dekker.

ZIEREP, J. 1969 Schallnahe strömungen mit wärmezufuhr. *Acta Mechanica* **8**, 126–132.

ZIEREP, J. 1971 *Similarity Laws and Modeling*. Marcel Dekker.